Development/Plasticity/Repair

Klf5 Regulates the Transition from Apical Radial Glia to Intermediate Progenitor Cells in the Developing Mammalian Brain

Takahiro Fuchigami,[1]* Yoshitaka Hayashi,[1]* Anri Kuroda,[1]* Zakiyyah Munirah Mohd Zaki,[1] Nur Azrah Fazera Mohd Ariffin,[1] Kenny Anak Daun,[1] Naoko Morimura,[1] Hiroaki Kitagawa,[1] Takuya Azami,[2] Shoji Tatsumoto,[3] Yasuhiro Go,[3,4,5] Kazuhiko Uchida,[6,7] Satoru Takahashi,[8,9] Kazuhiko Nakabayashi,[10] Masatsugu Ema,[2] and Seiji Hitoshi[1]

[1]Department of Integrative Physiology, Shiga University of Medical Science, Otsu 520-2192, Japan, [2]Research Center for Animal Life Science, Shiga University of Medical Science, Otsu 520-2192, Japan, [3]Cognitive Genomics Research Group, Exploratory Research Center on Life and Living Systems, National Institutes of Natural Sciences, Okazaki 444-8585, Japan, [4]Division of Behavioral Development, Department of System Neuroscience, National Institute for Physiological Sciences, National Institutes of Natural Sciences, Okazaki 444-8585, Japan, [5]Graduate School of Information Science, University of Hyogo, Kobe 650-0047, Japan, [6]Department of Molecular Biological Oncology, Institute of Basic Medical Sciences, Graduate School of Comprehensive Human Sciences, University of Tsukuba, Tsukuba 305-8577, Japan, [7]Institute for Biomedical Research, MCBI, Tsukuba 300-2635, Japan, [8]Department of Anatomy and Embryology, Institute of Medicine, University of Tsukuba, Tsukuba 305-8577, Japan, [9]International Institute for Integrative Sleep Medicine (IIIS), Transborder Medical Research Center (TMRC) and Laboratory Animal Resource Center (LARC), University of Tsukuba 305-8577, Tsukuba, Japan, and [10]Department of Maternal-Fetal Biology, National Research Institute for Child Health & Development, Tokyo 157-8535, Japan

Krüppel-like factors (Klfs) are DNA-binding transcriptional factors that regulate multiple physiological features, including the cell cycle, cell differentiation, and tissue organization. Among them, Klf2, Klf4, and Klf5 are crucial for the induction and maintenance of pluripotent stem cells. However, the roles of these factors in maintaining neural stem cells (NSCs) remain poorly understood. Here, we show that Klf5 plays a dominant role in maintaining neural precursor cell (NPC) populations by suppressing their differentiation and radial migration in developing mouse brains of either sex. Klf5 also regulates the proliferation of NPCs and promotes differentiation of Pax6$^+$ apical radial glia in the ventricular zone to Eomes$^+$ (Tbr2$^+$) intermediate progenitor cells in the subventricular zone by upregulating *Hes1* and *Eomes* expression. Overexpression of *Klf5* in NPCs reduced the pool of quiescent NSCs in the postnatal brain, resulting in attenuated neurogenesis in the subependymal zone and the dentate gyrus of the hippocampus in the adult brain. *Klf5*-overexpressing male mice exhibited impaired memory formation and reduced preference for social novelty. Our findings suggest a mechanism by which NPCs expand the output of differentiating cells through intermediate progenitor populations.

Key words: **intermediate progenitor cell; neural stem cell; neurosphere; notch signaling; radial glia; radial migration**

Significance Statement

Neural precursor cells (NPCs) in the mammalian developing brain take one of two fates: a few NPCs elongate their cell cycle time and become quiescent neural stem cells, whereas the others differentiate into intermediate progenitor cells. However, the molecular mechanisms underlying this fate choice remain largely unknown. The number of divisions of intermediate progenitor cells is much larger in primates than in rodents, providing a cellular basis for the expansion of the outer subventricular zone and for the massive production of neurons and glia in the primate brain, leading to gyrification of the primate cortex. In this study, we investigated the role of *Klf5* in the generation and proliferation of intermediate progenitor cells.

Received March 24, 2025; revised Feb. 26, 2026; accepted March 20, 2026.

Author contributions: S.H. designed research; T.F., Y.H., A.K., Z.M.M.Z., N.A.F.M.A., K.A.D., N.M., H.K., T.A., S. Tatsumoto, Y.G., K.U., S. Takahashi, K.N., M.E., and S.H. performed research; T.F., A.K., N.M., M.E., and S.H. analyzed data; S.H. wrote the paper.

We thank Dr. Ryoichiro Kageyama (Kyoto University) for Nestin-Cre mice. We also thank all staff of the Research Center for Animal Life Science and Central Research Laboratory for their technical support. This work was supported by Grants-in-Aid for Scientific Research (B; 16H04671; S.H.), for Scientific Research (C; 20K07758; Y.H.) and for Young Scientists (21K15007B; A.K.) from the Ministry of Education, Culture, Sports, Science and Technology of Japan and a grant from SENSHIN Medical Research Foundation (S.H.).

*T.F., Y.H., and A.K. contributed equally to this work.

The authors declare no competing financial interests.

Correspondence should be addressed to Seiji Hitoshi at shitoshi-tky@umin.ac.jp.

This paper contains supplemental material available at: https://doi.org/10.1523/JNEUROSCI.0584-25.2026

https://doi.org/10.1523/JNEUROSCI.0584-25.2026

Introduction

Genes for Krüppel-like factor (*Klf*) are orthologs of the *Drosophila melanogaster* gene Krüppel. They are critical regulators in cell proliferation and differentiation in mammalian development (Ghaleb et al., 2005; Suske et al., 2005; McConnell et al., 2007; Yamane et al., 2018). Klf protein family members, which share three C_2H_2 zinc-fingers at their carboxyl termini, are classified into subgroups based on their structural or functional relationships (Moore et al., 2011; Tetreault et al., 2013). Klf2 and Klf4 belong to the same subfamily, harboring a repression domain adjacent to an activation domain and nuclear localizing signals neighboring their first zinc finger domain (Bialkowska et al., 2017). Despite the fact that Klf5 is structurally divergent from Klf2 and Klf4, these three factors share common functions in the maintenance of cellular pluripotency (Bruce et al., 2007; Jiang et al., 2008; Nandan and Yang, 2009; Bourillot and Savatier, 2010). Whereas simultaneous depletion of *Klf2*, *Klf4*, and *Klf5* results in differentiation of embryonic stem cells (ESCs), overexpression of any one of three genes can achieve leukemia inhibitory factor-independent maintenance of pluripotent mouse ESCs (Jiang et al., 2008; Jeon et al., 2016). *Klf2*, *Klf4*, and *Klf5* also play important roles in neural development and neurogenesis (Moore et al., 2011). *Klf4* is expressed in neural stem cells (NSCs) but drastically downregulated in differentiated neurons during brain development. *Klf4* overexpression inhibits NSC proliferation that is accompanied by elevated glial fibrillary acidic protein (GFAP) expression and astrocyte hypertrophy, but the function of *Klf5* in the maintenance of the neural precursor cell (NPC) population remains largely unknown.

Fibroblast growth factor 2 (FGF2)-responsive NSCs are generated at Embryonic Day (E)8.5 in the mouse forebrain, and their population size expands during early embryonic stages (Hitoshi et al., 2004). During neural development, self-renewing NSCs assume a morphology of $Pax6^+$ apical radial glia that proliferate in the ventricular zone (VZ) and then migrate to the subventricular zone (SVZ), where they lose apical processes to become $Pax6^+$ outer radial glia. The presence of these cells, which was first recognized in the fetal brain of primates, was also later found in rodents (Hansen et al., 2010; Wang et al., 2011; Hevner, 2019). $Tbr2^+$ intermediate progenitors are a transit amplifying cell population in the SVZ and the source of excitatory cortical projection neurons (Haubensak et al., 2004; Kowalczyk et al., 2009). Expansion of the outer SVZ, comprising outer radial glia and intermediate progenitors, is the cellular basis for production of large numbers of neurons as well as the gyrification of the cortex in human and macaque monkey brains (Molnár et al., 2019). A few NSCs are selected and have elongated cell cycles as slowly dividing NSCs but other precursor cells vigorously proliferate to provide a massive volume of neurons and glia (Fuentealba et al., 2015; Furutachi et al., 2015; Tanaka et al., 2020). The molecular mechanisms underlying the segregation of slowly dividing and vigorously dividing NPCs remain largely unknown. In this study, we investigated the function of *Klf5* in neural development, focusing on the roles of *Klf5* in cell cycle regulation and in the maintenance of the NPC population.

Materials and Methods

Animals. All experiments were carried out with the permission of the institution's Animal Research Committee, and all mice used in these experiments were kept in the institution's Research Center for Animal Life Science with a 12:12 h light/dark cycle (lights on, 8:00 A.M.–8:00 P.M.) and *ad libitum* access to food and water. *Klf5* conditional knockout (cKO) and *Nestin-Cre* and CAG-stop-*Klf5* transgenic mice (Isaka et al., 1999; Ema et al., 2008; Azami et al., 2017) were maintained as heterozygous on either a CD1 or C57/BL6 background. E0.5 was defined as 2:00 P.M. on the day of plug detection. They were genotyped by PCR using primers described in each paper and in Table 1.

Generation of knockdown and expression vectors for Klf2, Klf4, *and* Klf5. Several target sequences were selected for each gene, and pairs of synthetic oligonucleotides were annealed and cloned into a pSilencer vector (Thermo Fisher Scientific), in which resultant shRNAs were transcribed under the control of the human U6 promoter. Target sequences used in this study are summarized in Table 1. *Klf2*, *Klf4*, and *Klf5* cDNAs were amplified by RT-PCR and cloned into pBR-CAG-cHA-pA vector (RIKEN DNA Bank).

RT-qPCR, RNA-sequencing, and microarray analysis. Total RNA was isolated using a RNeasy Mini kit (Qiagen), and 0.5–1.0 μg of total RNA was reverse-transcribed with an oligo-dT primer (Invitrogen) and ReverTra Ace (Toyobo) to synthesize cDNA. Quantitative RT-PCR analysis using the Light-Cycler system (Roche) was carried out according to the manufacturer's protocol. The primers used in this study are summarized in Table 1. The RNA-sequencing libraries were prepared using the NEBNext Ultra Directional RNA Library Prep Kit for directional libraries (New England BioLabs) and the KAPA HTP Library Preparation Kits (KAPA Biosystems) according to the manufacturer's instructions. The libraries were sequenced using the Illumina HiSeq platforms. Raw sequence reads were aligned to the reference mouse genomes (GRCm38/mm10) by HISAT2 (Kim et al., 2015). Genome-wide expression levels were measured as a unit of transcripts per kilobase million (TPM) using StringTie (Pertea et al., 2015), and the number of reads was counted per gene per sample using HTseq-count within HTSeq (Anders et al., 2015). Finally, differentially expressed genes (DEGs) were identified by DESeq2 (Love et al., 2014). Gene Ontology (GO) analysis was performed on DEGs using the DAVID functional annotation tool (Sherman et al., 2022). RNA-seq data have been deposited into the GEO database with the accession number GSE222950.

cDNAs of wild-type and *Klf5* OE ESCs were amplified linearly and labeled with a Cy3- or Cy5-conjugated nucleotide. Hybridization

Table 1. Primers

Gene	Primer	Sequence
Genotyping PCR		
Nestin-Cre tg	Cre-P3	5′-AGGTTCGTTCACTCATGGA-3′
	Cre-P2	5′-AAATCCATCGCTCGACCAGTTTAGTTACCC-3′
Klf5 cKO	Klf5-deletion	5′-GTAATGGATGTGAACAGATTTGAGG-3′
	Klf5-WT allele 3′	5′-CGACATGTCTTCACTAAAGTCACTC-3′
	Klf5-loxP	5′-TATAATGTATGCTATACGAAGTTAT-3′
CAG-stop-*Klf5* OE tg	Klf5-A1	5′-CGATTCACAACCCAAATTTACC-3′
	Klf5-B2	5′-TGGCGCTTCATGTGCAGCGCGA-3′
RT-PCR		
Klf2	Klf2-Fw2	5′-GCGTACACACACAGGTGAGA-3′
	Klf2-Rv2	5′-GCACAAGTGGCACTGAAAGG-3′
Klf4	Klf4-Fw	5′-TACCCCTACACTGAGTCCCG-3′
	Klf4 Rv	5′-GGAAAGGAGGGTAGTTGGGC-3′
Klf5	Klf5-A1	5′-CGATTCACAACCCAAATTTACC-3′
	Klf5-B1	5′-GTATGAGTCCTCAGGTGAGCTTTTA-3′
Hes1	Hes1-A2	5′-AGCGCACCCTGCAAGTTGGGCA-3′
	Hes1-B2	5′-TCAGAAGAGAGAGGTGGGCTAG-3′
Eomes	Tbr2-A1	5′-GCAAAGCGGACAATAACATGCA-3′
	Tbr2-B1	5′-GAGTCTTGGAAGGTTCATTCAA-3′
β-actin	β-actin-A1	5′-AGGCCAACCGTGAAAAGATGAC-3′
	β-actin-B1	5′-GTACATGGTGGTACCACCAGAC-3′
shRNA hairpin sequences		
Klf2	#1; 5′-GCCTTGTGAGAAATGCCTTTGAttcaagagaTCAAAGGCAT TTCTCACAAGGC-3′	
Klf4	#2; 5′-GCGCTACAATCATGGTCAAGTttcaagagaACTTGACCAT GATTGTAGCGC-3′	
Klf5	#2; 5′-GACGTCAATGAAACAGTTCttcaagagaGAACTGTTT CATTGACGTC-3′	

procedures were performed by TaKaRa Bio. Raw data were analyzed using the GeneSpring software version 13.0 (Agilent Technologies). The raw probe intensities were background-subtracted, and the signal values were set to threshold level 10 and log2-transformed. Normalization was performed using a 75th percentile shift algorithm; data were then normalized using a baseline-to-median-of-all-samples algorithm. Transcripts were filtered for a twofold change relative to the median intensity across all samples. Microarray data have been deposited in the GEO database under accession GSE245044.

Luciferase reporter assay. The distal and proximal promoter regions of the *Hes1* gene and the first and second introns of the *Eomes* gene were PCR amplified and cloned into a luciferase reporter plasmid (PicaGene basic vector 2, Toyo Ink). FuGENE6 (Roche) was used to transfect Neuro2a cells with the luciferase reporter plasmid and an internal control Renilla luciferase reporter plasmid (Promega), in combination with the following expression plasmids: pBR-CAG, pBR-CAG-Klf2, pBR-CAG-Klf4, pBR-CAG-Klf5, and pBR-CAG-myc-NICD. Luciferase activities were determined using a Dual-Luciferase Reporter Assay System (Promega).

Antibodies. Primary antibodies used in this study were as follows: rabbit anti-Klf5 (1:100, Abcam), rabbit anti-Pax6 (1:1,000, Millipore), rabbit anti-Tbr2 (1:1,000, Abcam), mouse anti-βIII tubulin monoclonal IgG (1:1000, Sigma-Aldrich), mouse anti-BrdU monoclonal IgG (1:1,000, Millipore), and rabbit polyclonal (1:2,000, Invitrogen) and rat monoclonal anti-GFP IgG (1:1,000, Nacalai Tesque) antibodies. We also used biotinylated goat anti-rabbit or anti-rat IgG antibodies (Vector Lab) and appropriate Alexa Fluor-conjugated secondary antibodies (1:4,000, Invitrogen).

Immunohistochemistry. Timed pregnant mice were intraperitoneally injected with BrdU [Sigma-Aldrich; 50 mg/kg dissolved in D-phosphate-buffered saline (PBS) at 10 mg/ml] 2 h before being killed. Embryos at E14.5 or older were transcardially perfused with 4% paraformaldehyde. Brains were harvested and postfixed with the same fixative overnight, followed by cryoprotection with 20% sucrose in PBS at 4°C. Coronal cryosections were cut at 10 μm thickness for E10.5 embryos or at 14 μm thickness for brains from E14.5 or E16.5 embryos using a cryostat (CM3050, Leica). Sections were permeabilized with 0.3% Triton X-100/PBS for 5 min and blocked with 10% normal goat serum/PBST for 1 h and then incubated with primary antibody overnight at 4°C. After washing with PBS, sections were incubated with a fluorescent-conjugated secondary antibody, followed by counterstaining of nuclei with Hoechst 33342 (1 μg/ml). For double immunostaining of GFP and BrdU, Tbr2 or Pax6, sections were stained with rabbit or rat anti-GFP antibodies, followed by biotinylated anti-rabbit/rat IgG antibody (1:200). Then, the sections were boiled in 10 mM citrate buffer, pH 6.0, for 5 min, blocked with 10% normal goat serum/PBS for 1 h, and reacted with primary antibodies for BrdU, Tbr2, or Pax6 at 4°C overnight. After washing, the sections were incubated with Alexa Fluor 488-conjugated streptavidin and Alexa Fluor 594-conjugated anti-mouse/rabbit IgG antibodies. For the immunostaining of Klf5, sections were incubated with 1.5 N HCl at 37°C for 20 min to retrieve epitopes. Sections were then sequentially incubated with blocking solution, anti-Klf5 antibody, biotinylated anti-rabbit IgG antibody, and Alexa Fluor 488-conjugated streptavidin. Fluorescence was visualized using an Olympus BX51 microscope with an Olympus DP70 CCD camera. Confocal images were captured using a laser-scanning microscope (SP8; Leica). Coronal sections for Nissl staining were cut at 10 μm thickness from paraformaldehyde-fixed, paraffin-embedded brains.

In situ hybridization. Synthesis of single-stranded riboprobes and in situ hybridization procedures were described previously (Ishino et al., 2014). Briefly, digoxigenin (DIG)-labeled single-stranded riboprobes for *Hes5* were synthesized using T3 RNA polymerase and DIG RNA labeling mix (Roche). The hybridized DIG-labeled probe was detected by overnight incubation of the sections with anti-DIG antibody conjugated to alkaline phosphatase (1:2,000; Roche). The color was developed in the presence of 4-nitro blue tetrazolium chloride, 5-bromo-4-chloro-3-indolyl phosphate (Roche).

In utero electroporation. In utero electroporation was performed as described previously (Naruse et al., 2006). GFP and shRNA expression plasmids at a concentration of 3.0 μg/μl in D-PBS containing 0.05% Fast Green were prepared immediately before use. Timed pregnant ICR mice at E13.5 were deeply anesthetized by intraperitoneal injection of 100 mg/kg ketamine (Daiichi Sankyo) and 10 mg/kg xylazine (Bayer) solution. An electroporator (CUY21, NEPA GENE) was used to deliver five 50 ms pulses of 32 volts at 950 ms intervals after plasmid DNA was microinjected into the lateral ventricles of the embryos, using a heat-pulled capillary pipette. To detect proliferating cells, BrdU (50 mg/kg body weight, Sigma-Aldrich) was injected intraperitoneally into the dam 2 h before the perfusion.

NPC culture. The isolation of NSCs from embryonic brains was performed as described previously (Tropepe et al., 1999; Hitoshi et al., 2011). To obtain primary neurospheres, cells from the ganglionic eminence of E15.5 embryos were dissociated into single cells and cultured at 10 cells/μl in serum-free medium [SFM; DMEM/F12 (1:1), 5 mM HEPES buffer, 0.6% glucose, 3 mM $NaHCO_3$, 2 mM glutamine, 25 μg/ml insulin, 100 μg/ml transferrin, 20 nM progesterone, 60 μM putrescine, and 30 nM sodium selenite] in the presence of 10 ng/ml FGF2 together with 2 μg/ml heparin (all from Sigma-Aldrich). NSCs from adult brains were isolated and cultured as described previously (Hitoshi et al., 2011). Briefly, brains were aseptically collected into oxygenized artificial cerebrospinal fluid (124 mM NaCl, 5 mM KCl, 1.3 mM $MgCl_2$, 2 mM $CaCl_2$, 26 mM $NaHCO_3$, 0.18% glucose, and 100 units/ml penicillin–streptomycin). The entire subependymal zone of the lateral ventricles was excised and cut into small pieces. The tissue was subjected to enzyme digestion in a solution containing 1.33 mg/ml trypsin, 0.67 mg/ml hyaluronidase, and 0.2 mg/ml kynurenic acid (all from Sigma-Aldrich) for 1 h at 37°C to facilitate tissue dissociation. The tissue was then triturated using a fire-polished Pasteur pipette in SFM containing trypsin inhibitor (Roche). After washing with SFM, the cells were cultured at a density of 5 cells/μl in a 24-well plate (Falcon) in 500 μl SFM containing 20 ng/ml EGF, FGF2, and heparin. The number of floating spherical colonies (neurospheres) was counted after 7 d when the sphere diameter exceeded 0.08 mm. The total number of neurosphere-forming NSCs in the adult brain was calculated based on the volume in which the SVZ cells were suspended (usually 600 μl), the volume applied in the culture, and the number of resultant neurospheres in the culture.

To assess self-renewal, primary single neurospheres were mechanically dissociated into single cells in 0.2 ml of SFM containing FGF2, EGF, and heparin and then subcloned in 96-well (0.2 ml/well) plates (Falcon). Self-renewal of NSCs was assessed by identifying new neurospheres after further culture for 7 d in vitro.

The cortices of E14.5 *Klf5* OE and littermate control embryos were treated with trypsin and DNase I at 37°C for 5 min before trituration into single cells. The cells (1.0×10^5) were cultured in 100 μl 5% B27/Neurobasal medium on a polyethyleneimine (0.1% in 0.15 M borate buffer), pH 8.4/Matrigel-coated cover glass. After 48 h, the cells were cultured in the presence of 5 μM BrdU for 4 h and in the presence of 5 μM BrdU/EdU for an additional 1 h. The cells were then fixed and immunostained for GFP and BrdU, followed by visualization of EdU using a Click-iT EdU Cell Proliferation Kit (C10337, Thermo Fisher Scientific) according to the manufacturer's protocol.

Single-cell RNA-sequencing and ChIP-sequencing data reanalysis. Single-cell RNA-seq and ChIP-seq data were downloaded from the GEO under the indicated accession numbers: single-cell GSE138243 (Belenguer et al., 2021) and ChIP-seq Klf4, SRR952210, and Klf5, SRR952211 (Aksoy et al., 2014). Downloaded FASTQ data were mapped to the *Mus musculus* genome (mm10) using HISAT2 (Kim et al., 2015). For single-cell RNA-seq, mapped reads were counted and annotated based on the *Mus musculus* genome assembly GRCm38 (mm10) using featureCounts (Liao et al., 2014). Following the original report, gene-level and transcript counts were then imported into the R/Bioconductor package edgeR (Chen et al., 2016) and were normalized for TMM (trimmed mean of M-values) to adjust for differences in library sizes. The false discovery rate (FDR) was calculated by EdgeR. For ChIP-seq, mapped reads

were converted to bigwig files using deepTools2 (Ramírez et al., 2016) to check the precipitated region by IGV (Robinson et al., 2023).

Magnetic resonance imaging. Magnetic resonance imaging (MRI) was performed as described previously (Amatsubo et al., 2009). Briefly, we used a 7.0 T horizontal-bore MR scanner (Unity Inova; Agilent Technologies) and obtained T2-weighted magnetic resonance images with parameters of TR/TE 1,800/42 ms with 0.8 mm intervals. The lateral ventricle size was measured by circumscribing the ventricles on T2-weighted images using ImageJ (https://imagej.net/software/imagej/). The total volume is the sum of the corresponding areas in square centimeter multiplied by the MR interplane gap of 0.8 mm.

Behavioral test. Behavioral tests were performed as described previously (Daun et al., 2020). The open-field test, Barnes maze test, social interaction test, and contextual and cued fear conditioning test were conducted according to the manufacturer's protocol (O'Hara & Co.). In the open-field test, the total distance was used as an index of locomotor activity in a novel environment. The number of times the animals reared was used to assess stereotypic behavior, and the percentage of time spent in the central area was used as an index of anxiety. Spatial memory was assessed using the Barnes maze test. After acquiring a memory for the target position, the target escape box was moved to a new position opposite the original one to assess memory renewal ability. Training trials were conducted on 8 consecutive days, and then the mice underwent a reversed probe trial. Conditioned fear memory was evaluated with contextual and cued tests that represented hippocampus-dependent and hippocampus-independent learning tasks, respectively. The contextual and cued fear conditioning tests were conducted 1, 7, and 28 d after the training to assess immediate, recent, and remote fear memory, respectively. One day after the remote memory testing, extinction training was performed on 4 consecutive days. Then, memory extinction was assessed 36 d after the initial training.

Sociability and social novelty preference assessment were conducted in a three-chamber social interaction apparatus with grid cages in the right and left chambers (O'Hara & Co.). Briefly, during a 10 min habituation period, when both grid cages were empty, the time spent around each grid cage by a subject mouse was measured. Following the habituation phase, a single, unfamiliar male mouse was placed in one of the two cages. Time spent around each grid cage was measured in a 10 min session as an indicator of sociability. Social novelty preference was evaluated in an additional 10 min session, during which a new, unfamiliar male mouse was placed in the previously empty grid cage.

Statistics. Statistical analysis was performed by one-way ANOVA followed by a Dunnett or Tukey honest significant difference test. If applicable, we used an unpaired two-tailed Student's *t* test. The level of significance was set at $p < 0.05$.

Results

Klf5 is dominant in the regulation of NPC migration, differentiation, and proliferation

We first examined expression levels of *Klf2*, *Klf4*, and *Klf5* by RT-qPCR in mouse ESCs and embryonic forebrain. Consistent with preceding studies (Bruce et al., 2007; Ema et al., 2008; Jiang et al., 2008; Parisi et al., 2008), we found abundant expression of these three genes in the ESCs (Fig. S1*A*). In the E8.5 forebrain as well as in the E14.5 cortex, expression levels were downregulated relative to the ESCs. *Klf5* exhibited expression levels several times higher than *Klf2* and *Klf4* in the developing brain ($F_{(2,6)} = 7.008$; $p = 0.0269$ for E8.5 forebrain; $F_{(2,6)} = 10.98$; $p = 0.0099$ for the E14.5 cortex by one-way ANOVA; Fig. S1*B*). Ubiquitous expression of Klf5 in the forebrain of E10.5 embryos and in the cortex and ganglionic eminence of E14.5 embryos was confirmed by immunohistochemistry (Fig. S1*C–E*).

To investigate the roles of *Klf2*, *Klf4*, and *Klf5* in neurogenesis, we performed in utero electroporation (Fig. 1*A*) to analyze the effects of acute knockdown and overexpression of each gene. We first electroporated shRNA-coding vectors together with a GFP expression plasmid into the dorsal VZ of embryos at E13.5. We analyzed the brains 72 h after the electroporation (Fig. 1*A*). Among *Klf2*, *Klf4*, and *Klf5*, only *Klf5* knockdown significantly enhanced the radial migration of NPCs to the cortical plate ($F_{(4,23)} = 4.585$; $p = 0.0141$; control vs *Klf5* KD; $p = 0.0052$ using a Dunnett multiple-comparisons test; Fig. 1*B*). Meanwhile, only *Klf5* overexpression suppressed the radial migration of NPCs ($F_{(3,14)} = 8.730$; $p = 0.0016$; control vs *Klf5* OE; $p = 0.0023$ using a Dunnett multiple-comparisons test; Fig. 1*C*,*D*). We also examined whether *Klf5* overexpression canceled the effect of *Klf5* knockdown, using a mutant form of *Klf5* (*Klf5*m). *Klf5*m carries nucleotide substitutions that makes it resistant to shRNA-mediated knockdown but generates no amino acid substitution relative to wild-type *Klf5*. We found that *Klf5*m indeed rescued the enhanced radial migration in the presence of *Klf5* shRNA expression ($F_{(2,13)} = 14.16$; $p = 0.0005$; pSilencer/pBR-CAG vs *Klf5* KD/pBR-CAG; $p = 0.0249$ and *Klf5* KD/pBR-CAG vs *Klf5* KD/*Klf5*m; $p = 0.0004$ using a Tukey multiple-comparisons test; Fig. 1*E*,*F*). These results suggest that *Klf5* suppresses the radial migration of NPCs. This, in turn, prompted us to examine differentiation because differentiation and radial migration of NPCs are tightly coupled.

$Pax6^+$ NPCs in the VZ are known to differentiate into $Tbr2^+$ SVZ cells. Contrary to our expectations, analysis of the brains 24 h after electroporation showed that *Klf5* overexpression increased the number of $Tbr2^+$ cells and decreased the number of $Pax6^+$ cells ($t_{(13)} = 2.750$; $p = 0.0165$ for $Tbr2^+$ cells; $t_{(13)} = 2.240$; $p = 0.0432$ for $Pax6^+$ cells; Fig. 2*A*,*B*). In addition, BrdU incorporation (50 mg/kg injected intraperitoneally 2 h before fixation) increased in the presence of *Klf5* overexpression ($t_{(17)} = 3.745$; $p = 0.0016$; Fig. 2*C*,*D*). These results suggest that *Klf5* facilitates the transition from $Pax6^+$ radial glia to $Tbr2^+$ intermediate progenitors but prevents further differentiation into neuroblasts.

Klf5 overexpression increases NPC proliferation and attenuates NSC self-renewal capability

We further determined the effects of *Klf5* overexpression in developing mouse brains by mating CAG-Stop-*Klf5* mice with mice carrying a NPC-specific Cre driver, *Nestin-Cre*, to generate *Nestin-Cre*, CAG-Stop-*Klf5* double transgenic (*Klf5* OE) mice (Fig. 3*A*). In *Klf5* OE mice, *Klf5* overexpression was induced in both the NPCs and their progeny. Immunohistochemical analysis of *Klf5* OE embryonic brains showed the presence of more $Tbr2^+$ cells in the VZ of *Klf5*-overexpressing brains compared with control mice (Fig. 3*B*). This observation was verified by a significant increase in the number of $Tbr2^+ Pax6^+$ cells among NPCs ($t_{(8)} = 2.616$; $p = 0.0308$; Fig. 3*C*). Furthermore, we found that *Klf5* overexpression enhanced proliferation of $Tbr2^+$ intermediate progenitor populations ($t_{(9)} = 3.413$; $p = 0.0077$; Fig. 3*D*). This observation suggested that terminal differentiation of $Tbr2^+$ intermediate progenitors was delayed due to augmented proliferation. Therefore, we conducted a birthdating analysis, in which NPCs were labeled with EdU at E11.5 and their destination was analyzed at P0. In the mammalian developing cortex, NPCs radially migrate and settle in an inside-to-outside pattern. Neurons in the deep layers are generated during the earliest stage of neurogenesis (E11.5–12.5). Indeed, we found that EdU^+ neurons were mostly present in layer VI/subplate of wild-type brains (Fig. 3*E*). In contrast, significantly more EdU^+ neurons were detected in layer V of the cortex of *Klf5* OE pups (Fig. 3*F*).

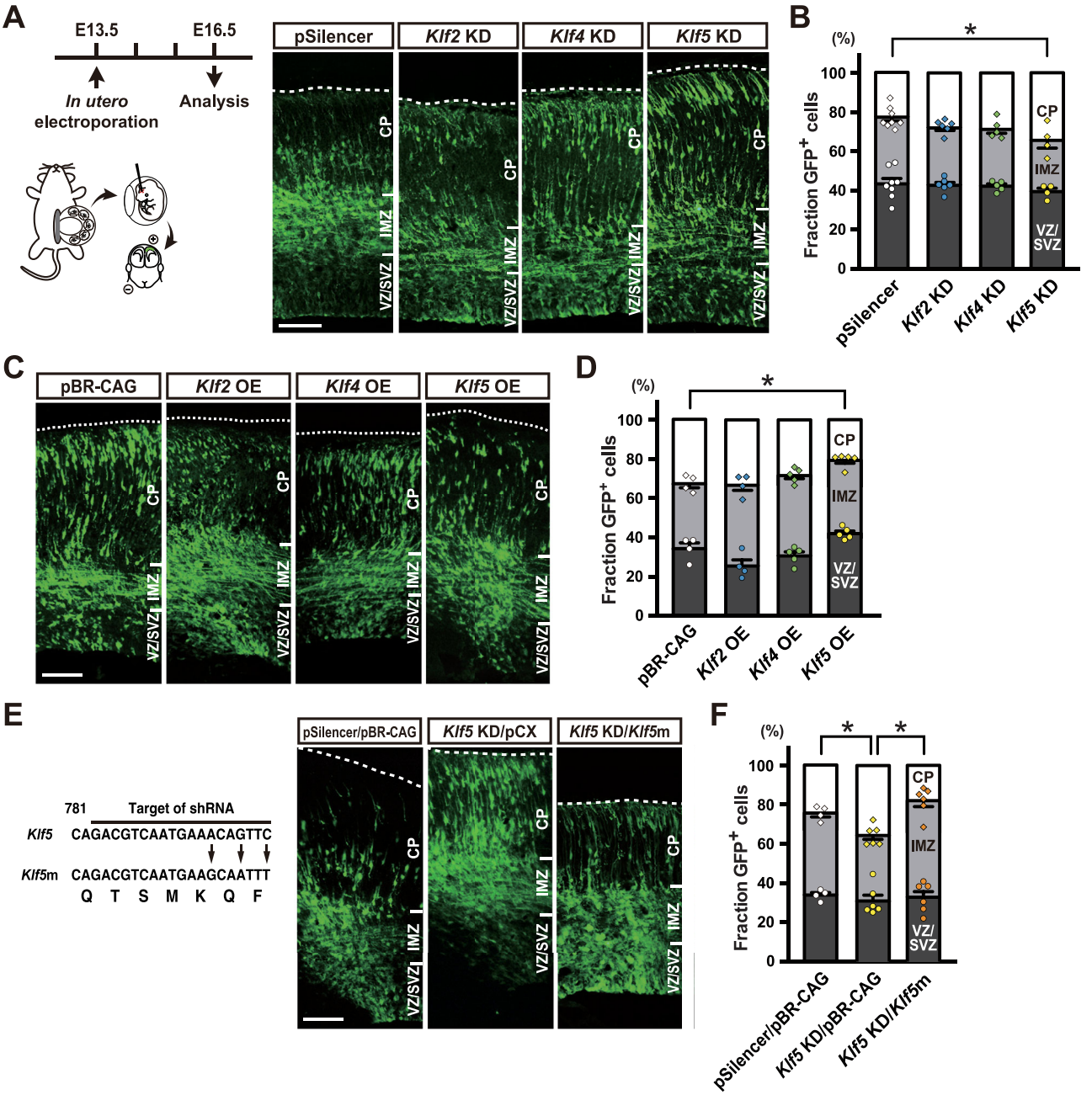

Figure 1. Effect of *Klf5* knockdown and overexpression on NPC migration. ***A***, Schematic diagram of in utero electroporation. At 72 h after in utero electroporation of shRNA plasmids for *Klf2*, *Klf4*, or *Klf5* together with pCX-EGFP into the cortex of E13.5 embryos, coronal cryosections were immunostained for GFP. White-dotted lines show the pial surface. ***B***, The percentage of GFP^+ cells in the cortical plate (CP, white), intermediate zone (IMZ, light gray), and VZ/SVZ (dark gray). ***C***, ***D***, *Klf2*, *Klf4*, or *Klf5* expression and control plasmids together with a pCX-EGFP expression plasmid were electroporated into the cortex of E13.5 embryos. The percentage of GFP^+ cells in the cortical plate was determined 72 h later. ***E***, Expression plasmid of a shRNA-resistant mutant form of *Klf5* (*Klf5*m, shown in the left scheme), together with *Klf5* shRNA and EGFP expression plasmids, were coinjected into the brains of E13.5 embryos and electroporated 72 h before immunostaining. ***F***, Percentages of GFP^+ cells. Circles and diamonds represent individual animals. Data were analyzed by one-way ANOVA, followed by a Dunnett (***B***, ***D***) or by Tukey (***F***) post hoc test ($*p < 0.05$), and are shown as means ± SEM. Scale bars, 100 μm.

In addition, we found that layers II–IV of the *Klf5* OE mouse cortex were thinner than those of the control cortex (Fig. 3*G*). These results suggest that the generation of early-born neurons was delayed and that production of late-born neurons was reduced in the cortex of *Klf5* OE pups. We also determined that $Olig2^+$ oligodendrocyte precursor cells were generated in the cortex and found that the percentage of $Olig2^+$ cells was increased in *Klf5* OE pup brains compared with control brains (Fig. 3*I*).

We next determined how *Klf5* overexpression affected cell cycle timing. We first showed that *Klf5*-transfected Neuro2a mouse neuroblastoma cells incorporated more BrdU than cells transfected with a control vector ($t_{(27)} = 5.243$; $p < 0.0001$; Fig. 4*A*,*B*). Then, we used a BrdU and EdU double labeling protocol to show that the average S-phase time and overall cell cycle time were both shorter in the presence of *Klf5* overexpression ($t_{(27)} = 3.921$; $p = 0.0005$ for Ts; $t_{(27)} = 9.444$; $p < 0.0001$ for Tc; Fig. 4*C*–*F*). We applied the same protocol to cells from the cortex of E14.5 *Klf5* OE and littermate control embryos (Fig. 5*A*). Consistent with the immunohistochemical results, more cortical cells from *Klf5* OE embryos incorporated BrdU than those from

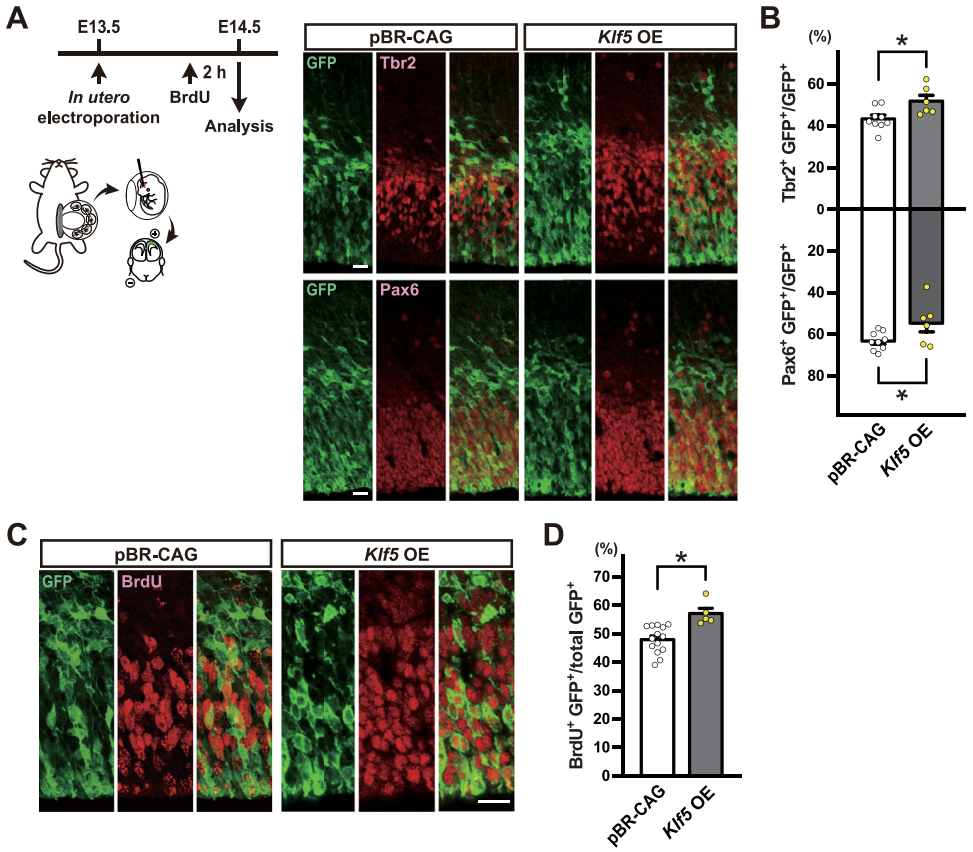

Figure 2. Effect of *Klf5* overexpression on NPC differentiation and proliferation. ***A***, ***C***, *Klf5* overexpression plasmid together with a pCX-EGFP expression plasmid was used for in utero electroporation into the cortex of E13.5 embryos. The brains were analyzed 24 h later. BrdU was intraperitoneally injected into the dam 2 h before sacrifice. Coronal cryosections were immunostained for GFP and either Tbr2 or Pax6 (***A***) or BrdU (***C***). ***B***, ***D***, Percentages of $Tbr2^+$ cells and $Pax6^+$ cells (***B***) and $BrdU^+$ cells (***D***) among GFP^+ cells after overexpression were calculated. Data were analyzed using Student's *t* tests (*$p < 0.05$) and are shown as means ± SEM. Scale bars, 20 μm.

control embryos ($t_{(12)} = 3.819$; $p = 0.0024$; Fig. 5*B*). At the same time, the average cell cycle time was shortened from 83.4 to 39.4 h in the presence of *Klf5* overexpression ($t_{(12)} = 2.855$; $p = 0.0145$; Fig. 5*C*).

Together, these results suggest that *Klf5* overexpression facilitates the transition from slowly dividing, neurosphere-forming NSCs to vigorously dividing neural progenitor cells, which remain undifferentiated but have lost self-renewal capability. Although some neural progenitor cells may form relatively small primary neurospheres in vitro, these primary neurospheres cannot be passaged to generate secondary neurospheres. We assessed the size of the neural precursor population by a colony-forming neurosphere assay using cells from the cortex of E13.5 embryos. We found that the number of primary neurospheres was increased in *Klf5* OE embryos compared with littermate wild-type embryos ($F_{(3,24)} = 6.059$; $p = 0.0032$; wild-type vs *Klf5* OE, $p = 0.0209$; Fig. 5*D*). It is possible that this increase resulted from enhanced proliferation of neural progenitor cells due to *Klf5* overexpression. We then evaluated the self-renewal capacity of neurosphere-forming cells by passaging single primary neurospheres, since the number of secondary neurospheres reflects the extent of symmetric, expansive divisions of NSCs during primary neurosphere formation. The number of secondary neurospheres was significantly reduced in *Klf5* OE embryos ($F_{(3,24)} = 3.108$; $p = 0.0453$; wild-type vs *Klf5* OE, $p = 0.0306$; Fig. 5*E*). NSCs in the cortex of mouse embryos migrate ventrally to the VZ of the ganglionic eminence and persist as quiescent, lifelong NSCs in the postnatal brain (Willaime-Morawek et al., 2006). Therefore, we also examined NSC self-renewal in the ganglionic eminence of E15.5 embryos. We found that the number of primary neurospheres was comparable among the genotypes, but the number of secondary neurospheres from *Klf5*-overexpressing NSCs was decreased compared with control NSCs ($F_{(3,31)} = 6.061$; $p = 0.0023$; wild-type vs *Klf5* OE, $p = 0.0008$; Fig. 5*F*,*G*). Thus, these results suggest that *Klf5* overexpression expands the $Tbr2^+$ neural progenitor population with reduced self-renewal capability.

Klf5 deficiency attenuates NSC self-renewal

We analyzed the effects of *Klf5* deficiency in developing mouse brains by mating *Nestin-Cre* tg and *Klf5* cKO mice (Fig. 6*A*). When proliferating cells were labeled with a 2 h exposure to BrdU, the ratio of $BrdU^+$ cells in the $Pax6^+$ population, but not in the $Tbr2^+$ population, was significantly lower in *Klf5* cKO than in control embryos ($t_{(4)} = 4.969$; $p = 0.0077$ for $Pax6^+$; $t_{(4)} = 0.914$; $p = 0.4125$ for $Tbr2^+$; Fig. 6*B*,*C*). We further examined the size of the NSC population in *Klf5* cKO embryos using cells from the ganglionic eminence of E15.5 embryos because ganglionic eminence NSCs exhibited much more self-renewal than cortical NSCs (Fig. 5*E*,*G*). We found that the number of primary neurospheres was significantly lower in E15.5 *Klf5* cKO than in littermate wild-type embryos ($F_{(2,35)} = 3.852$; $p = 0.0308$; control vs *Klf5* cKO; $p = 0.019$; Fig. 6*D*). In addition, the number of secondary neurospheres was significantly lower in the *Klf5* homozygous as well as heterozygous KOs than in wild-type primary neurospheres ($F_{(2,27)} = 4.909$; $p = 0.0152$; control vs *Klf5* heterozygous, $p = 0.0446$; control vs *Klf5* cKO, $p = 0.0136$; Fig. 6*E*).

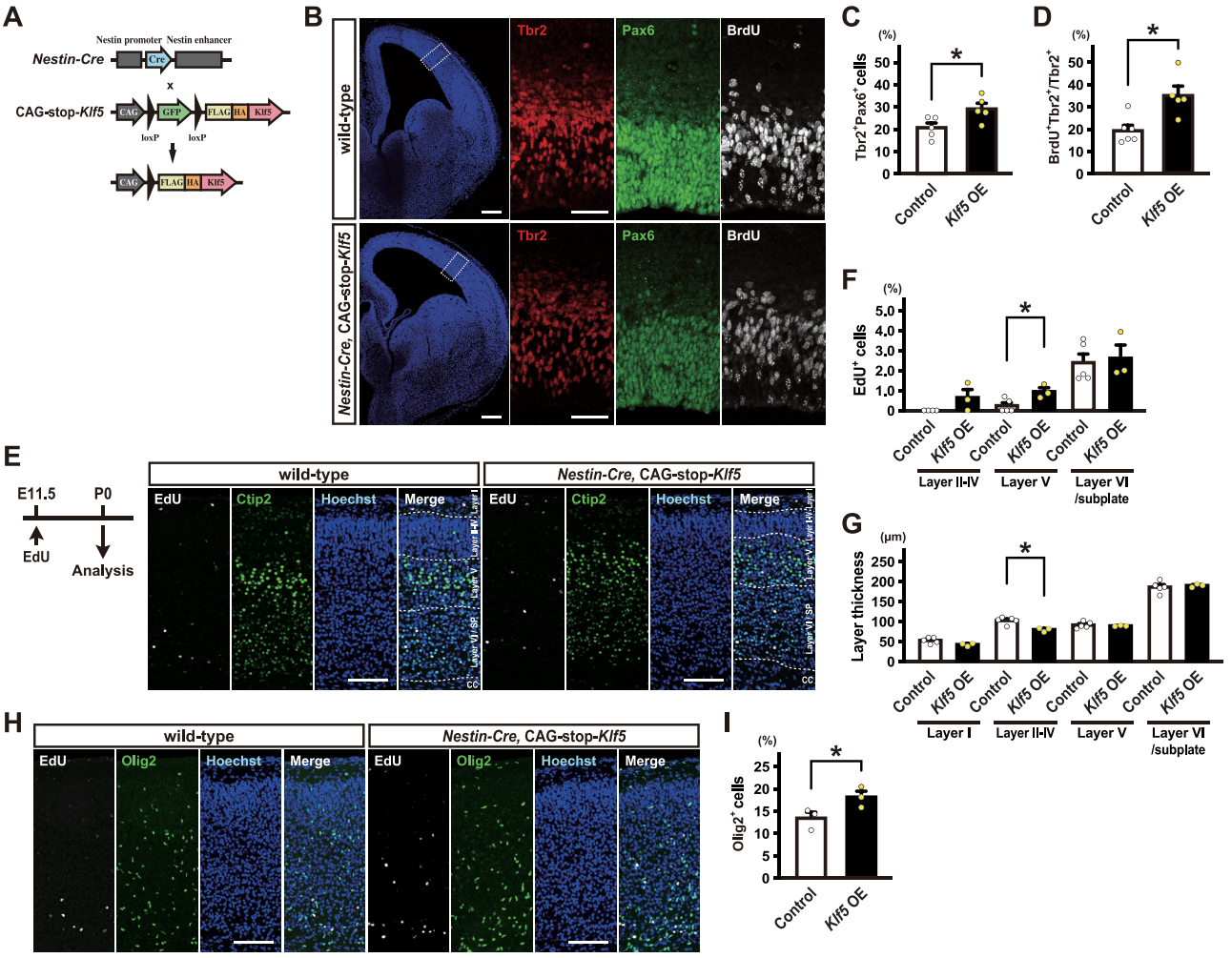

Figure 3. Analysis of *Klf5*-overexpressing mouse embryonic brains. ***A***, Generation of conditional *Klf5* overexpression (*Klf5* OE) mice by mating *Nestin-Cre* and CAG-Stop-*Klf5* transgenic mice. The CAG promoter drives *GFP* expression and FLAG/HA-tagged *Klf5* after Cre excision in the transgene. ***B***, BrdU was injected intraperitoneally into the dam at E14.5, and the embryos were perfused after 2 h. Coronal cryosections derived from *Klf5* OE or littermate wild-type embryos were triple immunostained for BrdU, Pax6, and Tbr2. Higher-magnification views of the areas enclosed by dotted squares are shown in the panels on the right. Scale bars, 200 μm (lower magnification) and 50 μm (higher magnification). ***C***, The percentage of $Tbr2^+Pax6^+$ cells in NPCs ($Tbr2^+$ or $Pax6^+$ cells). ***D***, The percentage of $BrdU^+Tbr2^+$ cells among all $Tbr2^+$ cells. ***E–I***, EdU was intraperitoneally injected into the dam at E11.5, and pups were perfused at P0. Coronal cryosections were immunostained for Ctip2 (***E***), a marker of layer V, or Olig2, a marker of oligodendrocyte-lineage cells (***H***), followed by visualization of EdU incorporation into DNA. Scale bars, 100 μm. ***F***, Percentages of EdU^+ cells in each layer of three sections at the level of the ganglionic eminence were counted and averaged. ***G***, Thickness of each layer at the medial, middle, and lateral regions of the cortex in three sections at the coronal level of the ganglionic eminence was measured and averaged. ***I***, Percentages of $Olig2^+$ cells in the cortex of three sections at the levels of ganglionic eminence were counted and averaged. Data were analyzed using Student's *t* tests (***C***, ***D***, ***F***, ***I***) or by one-way ANOVA followed by a Dunnett post hoc test (***G***) ($*p < 0.05$) and are shown as means ± SEM.

Thus, the self-renewal capability of NSCs was impaired by *Klf5* deficiency in a gene-dosage–dependent manner. These data appear inconsistent with the results of the *Klf5* overexpression study. However, this inconsistency disappears when Klf5 suppresses the differentiation of NPCs into postmitotic neurons, as demonstrated by *Klf5* KD experiments (Fig. 1*A*,*B*).

Downstream genes affected by *Klf5* overexpression in NPCs

RNA-sequencing analysis was carried out for primary neurospheres derived from the brain of *Nestin-Cre*::CAG-Stop-*Klf5* and *Nestin-Cre* control embryos. We identified 886 upregulated and 615 downregulated genes resulting from *Klf5* overexpression (Fig. 7*A*). The gene expression profiles clearly separated *Klf5*-overexpressing and control neurospheres (Fig. 7*B*). Consistent with the above notion, *Klf5* overexpression decreased the expression of *prominin 1*, a marker gene for stem cells (Florek et al., 2005; Walker et al., 2013; Fig. 7*A*). GO enrichment analysis for both up- and downregulated genes showed significant enrichment of biological processes related to NSC maintenance and Notch signaling (Fig. 7*C*). Notch signaling plays pivotal roles in the maintenance of NSCs (Artavanis-Tsakonas et al., 1995; Nakamura et al., 2000; Hitoshi et al., 2002; Yoon and Gaiano, 2005). We found that effector genes of Notch signaling, *Hes5* and *Hey1*, were downregulated, although another effector gene, *Hes1*, was at a high expression level; in contrast, Notch ligand genes, *Dll3* and *Jag1*, were upregulated in the *Klf5*-overexpressing neurospheres (Fig. 7*D*,*E*). *Klf2* and *Klf4* were not significantly affected by *Klf5* overexpression.

Recently, NPCs were analyzed by single-cell RNA-sequencing techniques to reveal distinct transcriptomic profiles in NSC populations (Llorens-Bobadilla et al., 2015; Belenguer et al., 2021). Thus, active NSCs in the subependymal zone of the adult mouse brain were characterized by a tendency for higher *Klf5* expression and significantly lower expression of *Klf2* and *Klf4* than those in

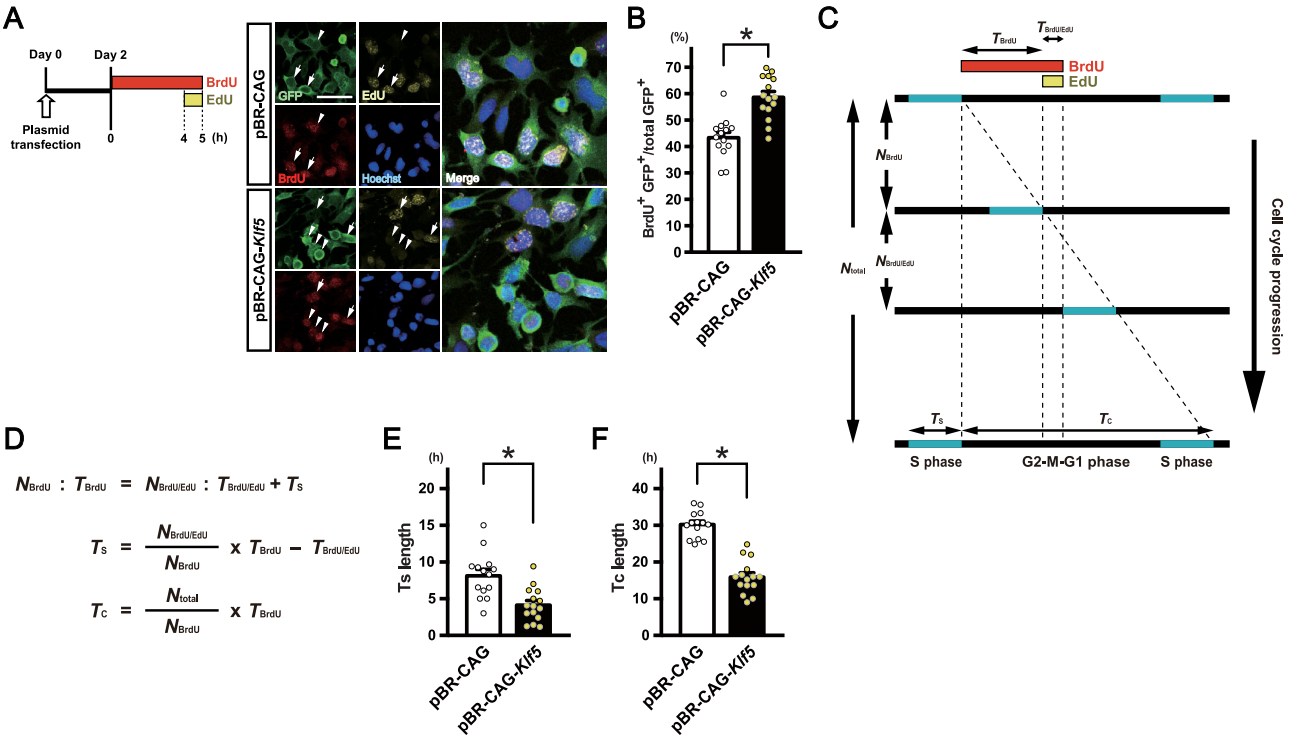

Figure 4. Shortening of the cell cycle time by Klf5 overexpression. ***A***, Schematic diagram of double labeling with BrdU and EdU. Neuro2a cells were transfected with Klf5 overexpression and control plasmids, together with a GFP expression plasmid. Two days after transfection, the cells were cultured in the presence of BrdU for 4 h, followed by BrdU/EdU for 1 h. The cells were then fixed and immunostained for GFP and BrdU, followed by visualization of the EdU reaction. White arrows and arrowheads indicate $BrdU^+EdU^+$ and $BrdU^+EdU^-$ cells, respectively. Scale bar, 50 µm. ***B***, Percentages of $BrdU^+$ cells among GFP^+ transfectants. ***C***, ***D***, Schematic diagram (***C***) and equations (***D***) for the calculation of S-phase time (Ts) and cell cycle time (Tc). ***E***, ***F***, S-phase time (***E***) and cell cycle time (***F***) of *Klf5*-transfected and control Neuro2a cells. Data were analyzed using Student's *t* tests (*$p < 0.05$), and error bars indicate means ± SEM.

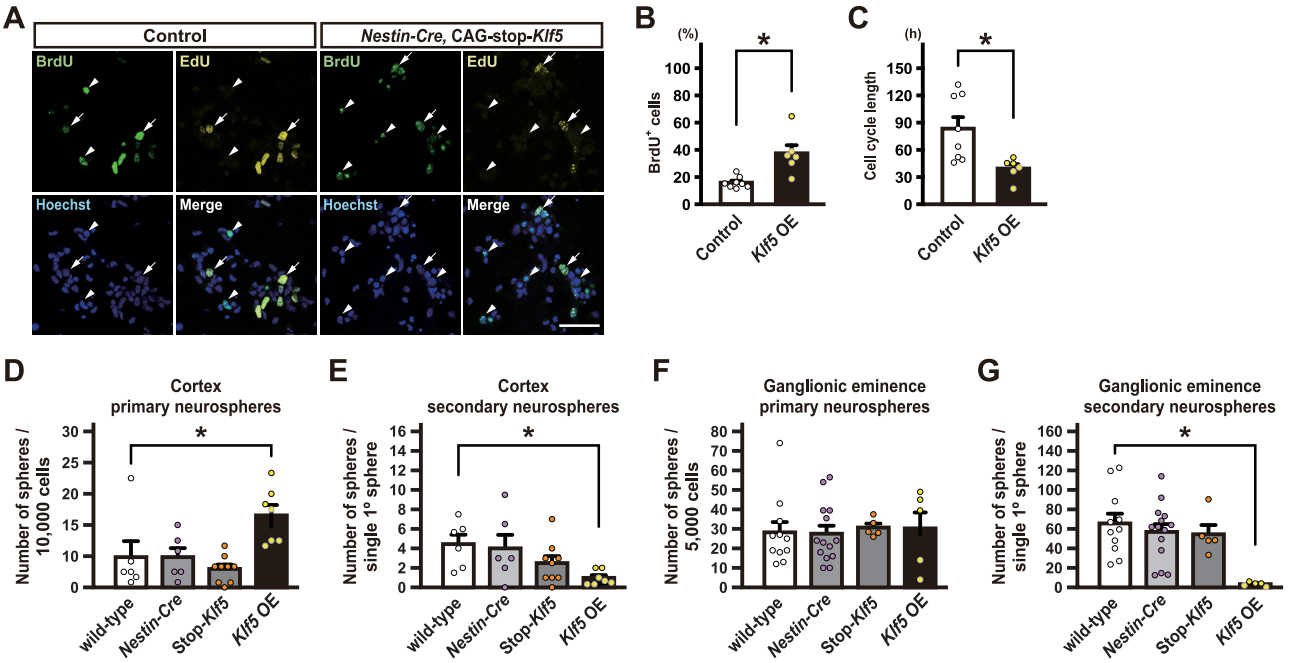

Figure 5. Cell cycle time and self-renewal of Klf5-overexpressing NPCs. ***A***, Cells from the cortex of E14.5 Klf5 OE and littermate control embryos were cultured in the presence of BrdU for 4 h and then in BrdU/EdU for 1 h. The cells were then fixed and immunostained for GFP and BrdU, followed by visualization of the EdU reaction. White arrows and arrowheads indicate $BrdU^+EdU^+$ and $BrdU^+EdU^-$ cells, respectively. Scale bar, 50 µm. ***B***, Percentages of $BrdU^+$ cells. ***C***, Average cell cycle times. ***D***, ***F***, Numbers of primary neurospheres derived from the cortex of E13.5 mouse brains (***D***) or from the ganglionic eminence of E15.5 mouse brains (***F***), which were cultured in SFM in the presence of FGF-2 and heparin for 7 d. ***E***, ***G***, Individual primary neurospheres were mechanically dissociated and recultured in SFM in the presence of EGF, FGF-2, and heparin. The number of secondary neurospheres derived from single primary neurospheres was counted after 7 d. Data were analyzed using Student's *t* tests (***B***, ***C***) or by one-way ANOVA, followed by a Dunnett post hoc test (***D–G***) (*$p < 0.05$) and are shown as means ± SEM.

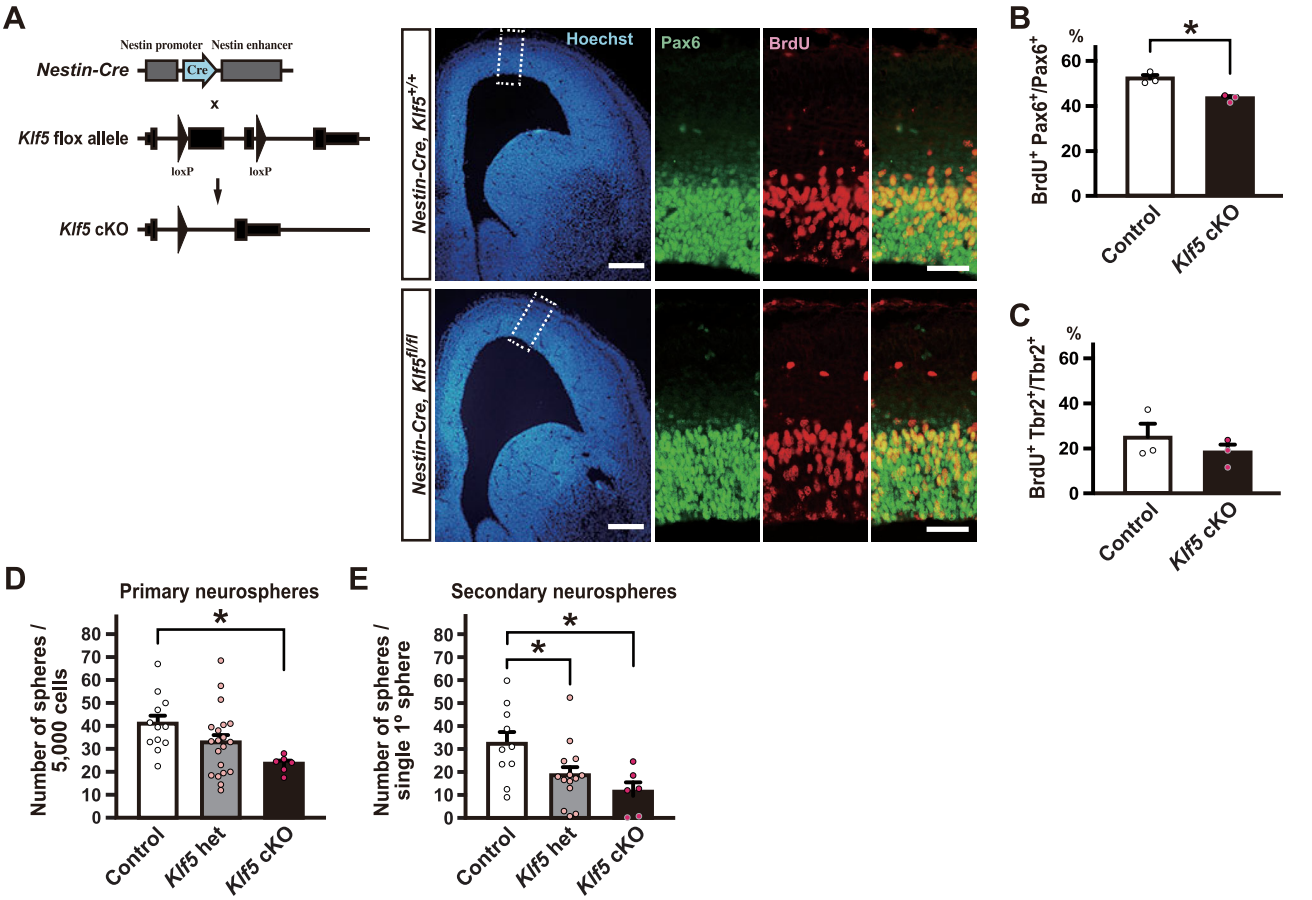

Figure 6. The self-renewal of *Klf5*-deficient NSCs. ***A***, NPC-specific *Nestin-Cre* driver mice were used to generate *Klf5* cKO embryos. BrdU was injected intraperitoneally into the dam at E14.5, and embryos were perfused after 2 h. Coronal cryosections derived from *Nestin-Cre* or *Nestin-Cre*, *Klf5* cKO embryos were double immunostained for Pax6 and BrdU. Scale bars, 200 μm (lower magnification) and 50 μm (higher magnification). ***B***, ***C***, Percentages of $BrdU^+Pax6^+$ cells in total $Pax6^+$ cells (***B***) and $BrdU^+Tbr2^+$ cells in total $Tbr2^+$ cells (***C***) were calculated. ***D***, Numbers of primary neurospheres derived from the ganglionic eminence of E15.5 embryos were counted. ***E***, Each primary neurosphere was mechanically dissociated and recultured in SFM in the presence of EGF, FGF-2, and heparin. The number of secondary neurospheres derived from single primary neurospheres was counted after 7 d. Data were analyzed using Student's *t* tests (***B*** and ***C***) or by one-way ANOVA, followed by a Dunnett post hoc test (***D*** and ***E***) ($*p < 0.05$) and are shown as means ± SEM.

shallow quiescent NSCs (Fig. 7*F*). Interestingly, active NSCs exhibited similar expression profiles for Notch signaling-related genes as those in *Klf5*-overexpressing neurospheres, except for *Hes1* (Fig. 7*F*).

The RNA-seq data and our microarray analysis using *Klf5*-overexpressing ESC lines detected 95 and 75 commonly upregulated and downregulated genes, respectively (Fig. 7*G*). Among them, *Hes1* expression in *Klf5*-overexpressing ESCs was increased by 1.53-fold compared with control ESCs ($n = 2$ for each group). The public ChIP-sequencing database for genomic binding of Klf5 in mouse ESCs showed that Klf5 preferentially occupies the promoter region of *Hes1* but not that of *Hes5* (Fig. 7*H*), suggesting that *Hes1* is a direct target of transactivation by Klf5. We tested this notion by measuring *Klf5* transcriptional activity using a firefly luciferase reporter assay in Neuro2a cells. When a distal region of the *Hes1* promoter where Klf5 ChIP-seq peaks accumulated was ligated to the luciferase gene, overexpression of Klf5, but not Klf2 or Klf4, significantly enhanced promoter activity compared with the control expression vector (Fig. S2*A*). In contrast, when the proximal region of the *Hes1* promoter, where an RBP-J binding site exists, was tested, only the Notch1 intracellular domain (NICD), the active form of the Notch1 receptor, produced strong promoter activity (Fig. S2*A*). Consistent with these findings, Klf5 and NICD overexpression induced *Hes1* expression in Neuro2a cells (Fig. S2*B*). No apparent peaks were observed in the promoters of *Dll3* or *Jag1* genes. In addition, we observed a moderate peak for Klf5 binding in the second intron of the *Eomes* (*Tbr2*) gene (Fig. 7*H*). Interestingly, *Eomes* expression was upregulated in the *Klf5*-overexpressing ESCs (average 3.13-fold change) relative to control ESCs, suggesting that Klf5 directly transactivates *Eomes* expression. Indeed, although we could not detect any promoter activity in the first and second introns of *Eomes* following Klf2, Klf4, or Klf5 expression, only Klf5 significantly increased *Eomes* expression (Fig. S2*C*,*D*). We further tested whether Klf5 overexpression specifically upregulates *Hes1* or *Eomes* expression in NPCs using Klf4- or Klf5-expressing lentivirus vectors (Fig. S3*A*–*C*). We confirmed that Klf5, but not Klf4, overexpression resulted in a significant increase in *Hes1* and *Eomes* expression in lentivirus-infected neurospheres (Fig. S3*D*,*E*).

Hes1 expression is normally restricted to $Pax6^+$ cells in the VZ (Fig. 7*I*), yet in brains from *Klf5*-overexpressing embryos some $Tbr2^+Pax6^-$ cells in the SVZ did express *Hes1* (Fig. 7*I*). Thus, these results support the notion that *Klf5* plays a key role in the generation of $Tbr2^+$ neural progenitors that lose their self-renewal capability and that *Klf5*-mediated *Hes1* upregulation prevents the cells from further differentiating into neuroblasts and maintains their proliferation as intermediate progenitors.

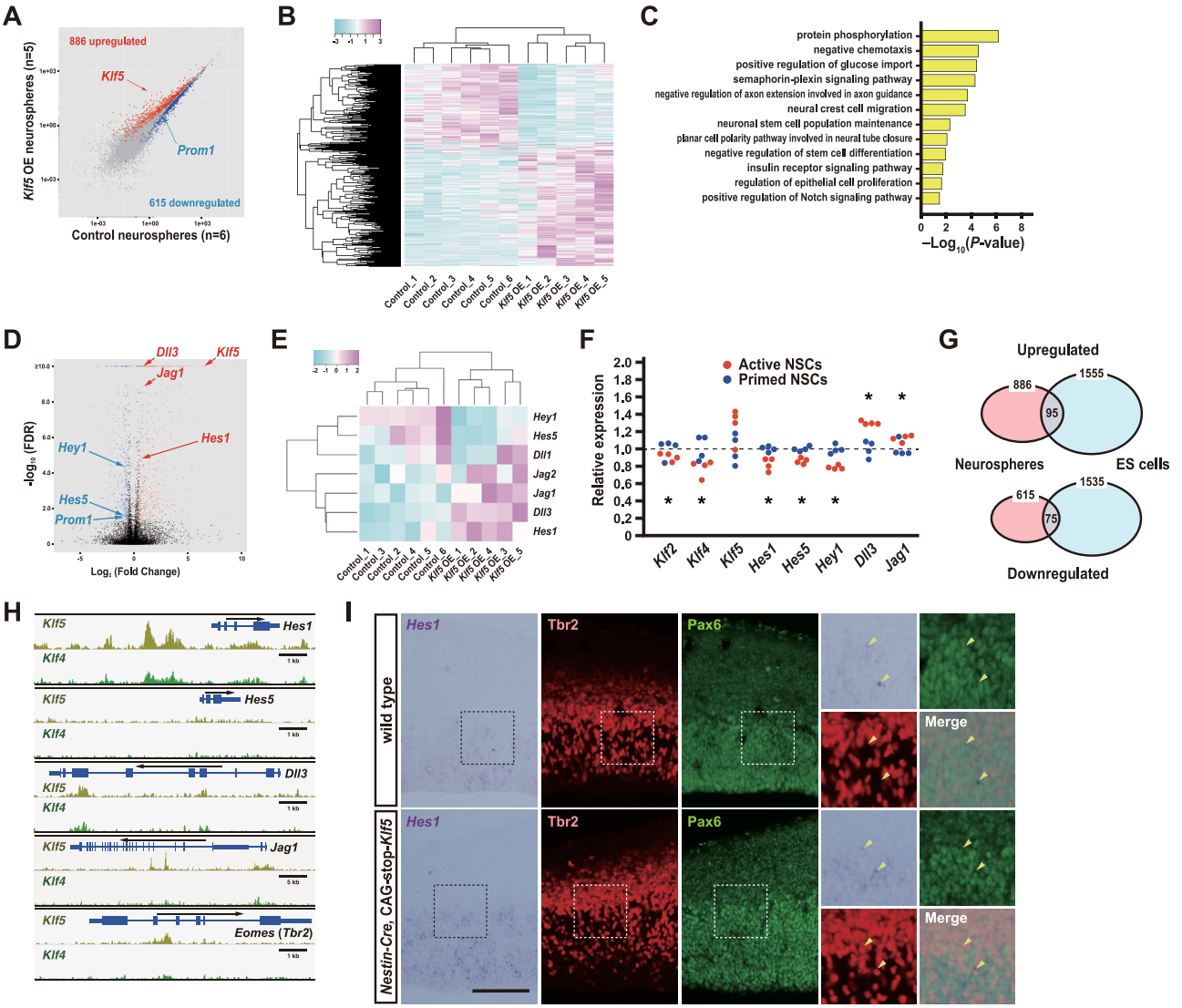

Figure 7. Transcriptome and ChIP-sequencing analyses of *Klf5*-overexpressing NPCs. ***A***, RNA-sequencing data shown as scatterplots comparing the global gene expression profile of primary neurospheres derived from E15.5 *Klf5* OE or *Nestin-Cre* littermate control embryos. Red and blue arrows point to yellow dots indicating *Klf5* and *prom1*, respectively. ***B***, Heat map showing expression levels of DEGs. ***C***, GO enrichment analysis for both up- and downregulated genes displayed as fold change in expression between *Klf5* OE and littermate control animals. ***D***, Volcano plot of DEGs. ***E***, Heat map showing expression levels of genes related to Notch signaling. ***F***, Relative single-cell expression levels normalized to the average of primed (shallow quiescent) NSCs. Asterisks indicate that the expression levels of the indicated genes in active NSCs are significantly upregulated or downregulated compared with primed NSCs (FDR < 0.05). ***G***, Venn diagram showing the number of upregulated and downregulated genes that are expressed in both *Klf5*-overexpressing neurospheres and ESCs. ***H***, Peaks for Klf5 and Klf4 binding to *Hes1*, *Hes5*, *Dll3*, *Jag1*, and *Eomes* (*Tbr2*) loci. ***I***, Codetection of *Hes1* expression using in situ hybridization followed by immunostaining for Tbr2 and Pax6 in the E15.5 cortex. Higher-magnification views of the areas enclosed by dotted squares are shown in the panels on the right. Arrowheads indicate representative cells containing in situ hybridization signals. Scale bars, 50 µm.

Klf5 overexpression results in ventriculomegaly and reduced adult neurogenesis

We further analyzed *Klf5* OE mice in the postnatal stages. First, we found that *Klf5* OE mice had smaller brains than their littermate controls ($t_{(18)} = 2.525$; $p = 0.0212$; Fig. 8*A*). MRI of the *Klf5* OE brains showed enlargement of the lateral ventricles ($t_{(4)} = 3.850$; $p = 0.0183$; Fig. 8*B*,*C*). This phenotype was likely not due to occlusion of cerebrospinal flow because we never observed tumor-like cell proliferation along and protrusions into the ventricular system that would have prevented the flow. This finding is likely attributable to cortical hypoplasia in *Klf5* OE mice and, therefore, is consistent with ex vacuo ventriculomegaly. Our observations of the neural precursor population in the embryonic brain indicate that *Klf5* overexpression facilitates the transition from Pax6$^+$ radial glia to Tbr2$^+$ intermediate progenitor cells and predict that the population of self-renewing NSCs will decrease in the postnatal brain. Indeed, the number of NSCs was depleted in 10-week-old *Klf5* OE mice compared with their littermate controls ($F_{(3,9)} = 22.46$; $p = 0.0002$; Fig. 8*D*), and the self-renewal capability of *Klf5*-overexpressing NSCs was drastically attenuated relative to control NSCs ($F_{(3,9)} = 10.33$; $p = 0.0028$; Fig. 8*E*). The total number of neurosphere-forming NSCs was substantially reduced in the *Klf5* OE mouse brain over the lifespan of the animal (Fig. 8*F*). Moreover, the degree to which the rate of neurosphere production was reduced was higher in *Klf5* OE mice than in control mice (by 43.82% from 10 to 24 weeks in *Klf5* OE mice vs 19.08% in control mice; Fig. 8*F*). As a result of this NSC depletion, the number of transit amplifying cells, the direct progeny of NSCs that can be detected by BrdU incorporation, was decreased in both the subependymal zone and subgranular zone of the dentate gyrus in *Klf5* OE mice relative to the littermate controls ($t_{(9)} = 3.010$; $p = 0.0147$ for the

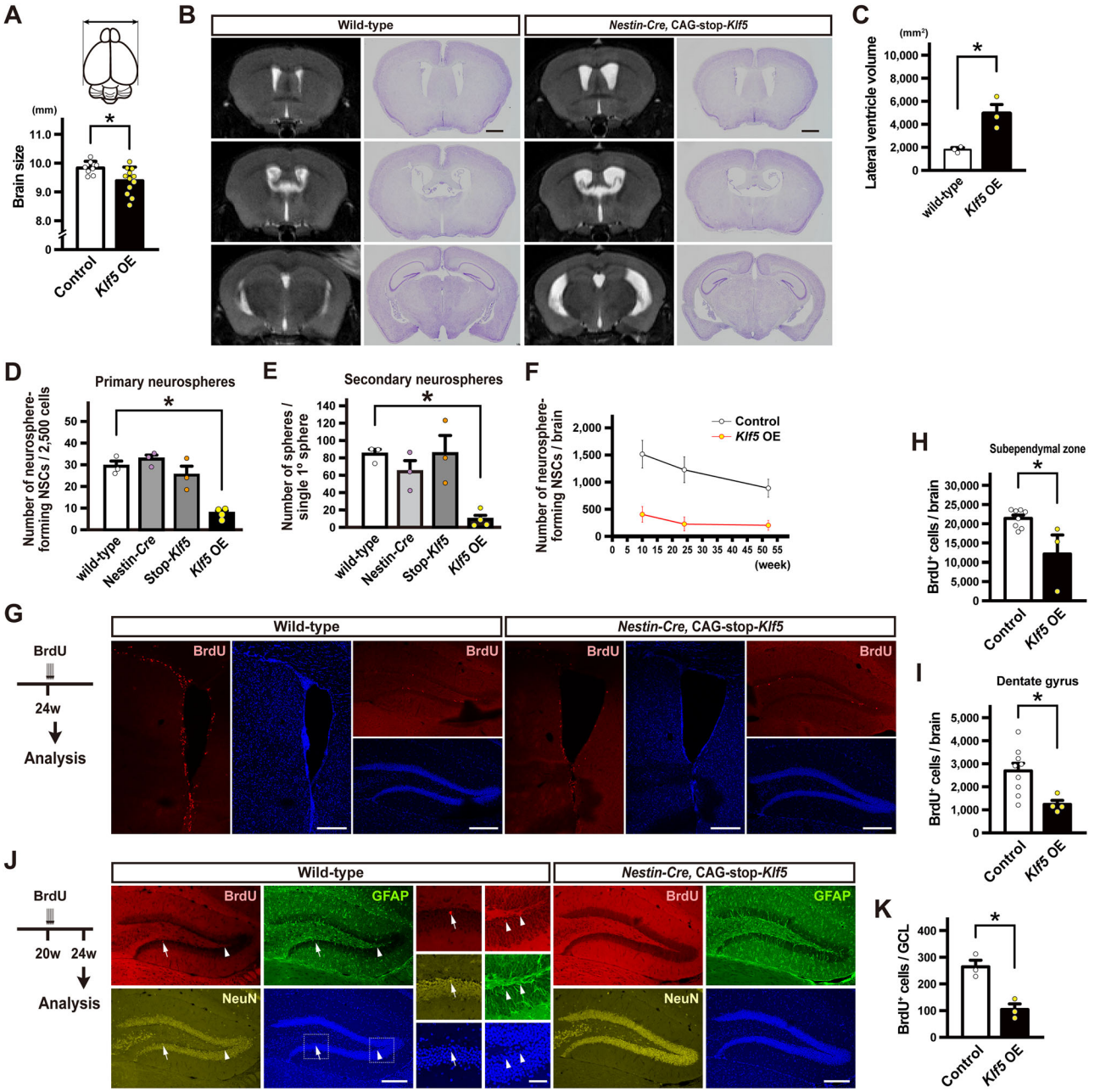

Figure 8. Analysis of postnatal mouse brains with *Klf5* overexpression. ***A***, The brain size as indicated by the illustration was measured in *Klf5* OE ($n = 8$) and littermate control mice ($n = 12$). ***B***, Representative T2-weighted magnetic resonance images and Nissl-stained sections of 10 week *Klf5* OE and littermate wild-type mouse brains. Coronal planes at the anterior commissure (top panels), the interventricular foramen (center panels), and the splenium (bottom panels) are shown. ***C***, The lateral ventricle size measured in *Klf5* OE ($n = 3$) and littermate wild-type mice ($n = 3$). ***D***, The number of resulting primary neurospheres counted after 2,500 cells from the tissue surrounding the lateral ventricles (the subependymal zone) of 10 week mouse brains were cultured for 7 d in SFM in the presence of EGF, FGF-2, and heparin. ***E***, The number of secondary neurospheres derived from single primary neurospheres that were mechanically dissociated and recultured in the same medium for 7 d. ***F***, The total number of neurosphere-forming NSCs in the brains of *Klf5* OE ($n = 4$–7 at each time point) and littermate control ($n = 7$–9 at each time point) mice over the lifespan of the animals. Data are shown as means ± SD. ***G***, BrdU (50 mg/kg) was intraperitoneally injected five times at 3 h intervals. The mice were killed 1 h after the last injection. Coronal cryosections of *Klf5* OE and littermate wild-type mice were immunostained for BrdU. ***H***, ***I***, Numbers of BrdU$^+$ cells in the subependymal zone (***H***) and in the dentate gyrus (***I***) of 24 week *Klf5* OE and littermate control mouse brains. ***J***, BrdU was intraperitoneally injected into mice five times at 20 weeks of age, and the mice were killed 4 weeks after the last injection. Coronal cryosections of *Klf5* OE and littermate wild-type mice were immunostained for BrdU and the indicated markers. Arrowheads and arrows indicate BrdU$^+$ cells in the subgranular zone and the granular cell layer (GCL), respectively. The areas within the dashed boxes are shown on the right at higher magnification. ***K***, The total number of BrdU$^+$ cells in the GCL from the rostral tip of the dentate gyrus to the end of the splenium of 24 week *Klf5* OE and littermate control mouse brains. Data were analyzed using Student's *t* tests (***C***, ***H***, ***I***, ***K***) or by one-way ANOVA, followed by a Dunnett post hoc test (***D***, ***E***) (*$p < 0.05$) and are shown as means ± SEM except for ***F***. Scale bars, 1 mm (***B***), 200 μm (***G***, ***J*** lower magnification), and 50 μm (***J*** higher magnification).

subependymal zone; $t_{(11)} = 2.800$; $p = 0.0173$ for the subgranular zone; Fig. 8*G*–*I*). We further determined neurogenesis in the granular cell layer by a long-term BrdU labeling study, in which NPCs in the subgranular zone were labeled at 20 weeks of age and analyzed for their differentiation into NeuN$^+$ mature neurons over 4 weeks (Fig. 8*J*). We observed a reduction in BrdU$^+$ neurons in the *Klf5* OE mice compared with littermate controls ($t_{(4)} = 4.887$; $p = 0.0081$).

We next tested if the reduction in the number of NSCs and subsequent neurogenesis affected the behavior of *Klf5* OE mice.

In an open-field test, *Klf5* OE mice showed hyperactive locomotion ($t_{(38)} = 2.592$; $p = 0.0135$) but had anxiety levels, as measured by the center time, that were comparable to those of the control mice (Fig. 9*A*). In a Barnes maze test to assess spatial memory, *Klf5* OE mice were less able to recall the position of the target escape box compared with control animals, although they did eventually acquire comparable memory to the control animals as assessed in a probe test ($t_{(34)} = 0.2347$; $p = 0.8159$; Fig. 9*B*,*C*). *Klf5* OE mice showed apparent memory impairment when the target escape box was moved to a new position opposite the original one ($t_{(34)} = 2.516$; $p = 0.0167$; Fig. 9*B*,*D*). In contrast, conditioned fear memory was grossly similar between *Klf5* OE and their littermate control mice in both a contextual and cued test, which are considered as hippocampus-dependent and

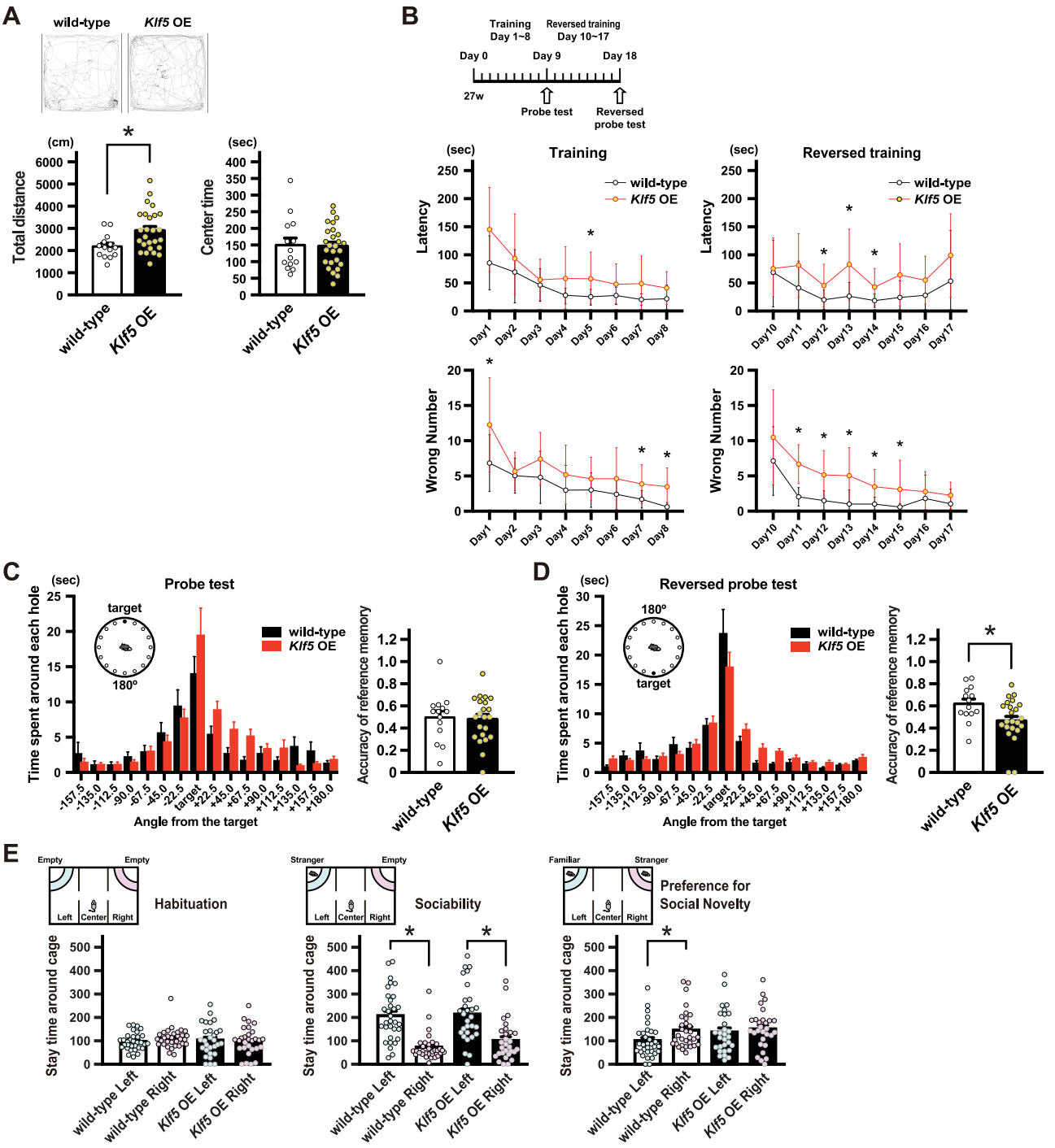

Figure 9. Behavior analysis of mice with *Klf5* overexpression. ***A***, *Klf5* overexpression (*Klf5* OE) and littermate wild-type male mice at 10 weeks of age were subjected to an open-field test. Representative trajectories in the open-field chamber during the 10 min test period are shown. Total traveled distance (left) and time spent in the center area (right) were compared. ***B***, *Klf5* OE ($n = 22$) and littermate wild-type ($n = 14$) male mice were assessed for spatial memory in a Barnes maze test. Latency and errors in entering the target escape box were measured during the training and reversed training. ***C***, ***D***, In the probe (***C***) and reversed probe (***D***) tests, time spent around each hole was measured in relation to the angle of the hole to the target. The accuracy of the reference memory was scored as the ratio of the time spent around the target to the time spent around the target and neighboring holes. ***E***, *Klf5* OE and littermate wild-type male mice were assessed for sociability and novelty preference in a three-chamber apparatus. After habituation training to the apparatus, the time spent around each grid chamber was measured. Data were analyzed using Student's *t* tests (***A***, ***C–E***) or by two-way ANOVA (***B***) (*$p < 0.05$) and are shown as means ± SEM except for ***B***, in which error bars indicate SD.

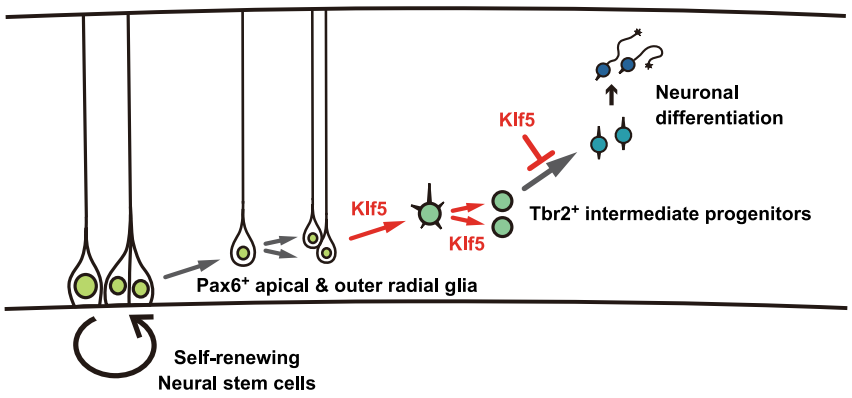

Figure 10. A model of Klf5 function in NPCs. Klf5 induces a transition from Pax6$^+$ apical and outer radial glia to Tbr2$^+$ intermediate progenitors and promotes proliferation of these cells, which, in rodents, normally divide at most once. At the same time, Klf5 suppresses further differentiation of these cells, leading to expansion of the intermediate progenitor population.

independent learning tasks, respectively (Fig. S4). Sociability and social novelty preference assessment conducted using a three-chamber social interaction apparatus revealed that *Klf5* OE and their littermate control mice had comparable interest in stranger mice ($F_{(3,118)} = 17.62$; $p < 0.0001$; sociability), indicating no preference for social novelty by *Klf5* OE mice (Fig. 9*E*).

Discussion

We demonstrated here that *Klf5* shares a common function with *Klf4* and suppresses the radial migration of NPCs to the cortical plate (Qin and Zhang, 2012). On the other hand, *Klf5* plays an opposite role to *Klf4* in the maintenance of the NPC population. *Klf4* inhibits the proliferation of NPCs and enhances expression of GFAP, a marker of NSCs in the postnatal brain (Qin and Zhang, 2012), whereas *Klf5* induces the transition from Pax6$^+$ radial glia to Tbr2$^+$ intermediate progenitors and increases their proliferation. Similar opposing effects of Klf4 and Klf5 on cell proliferation were documented using several cancer cell lines (Dang et al., 2003; Ohnishi et al., 2003; Nandan et al., 2008). Hence, *Klf4* and *Klf5* are considered to be tumor suppressive and pro-oncogenic genes, respectively. In normal neural development, NPC proliferation is tightly coupled with NSC lineage differentiation (Ishino et al., 2014). The demonstration of slowly dividing NSCs, which are selected from the NPC populations during early developmental stages (Fuentealba et al., 2015; Furutachi et al., 2015), raises a question about how those slowly dividing and vigorously dividing states in NPCs are regulated and how proliferation of neural progenitor cells is adjusted so that they produce appropriate numbers of neurons and glia in the postnatal brain. Results of our study support a molecular mechanism in which *Klf5* expression levels determine the fate of NPCs in the developing brain, such that the majority lose self-renewal capability and become intermediate progenitors that are consumed after an appropriate number of divisions as they generate neurons and glia (Fig. 10).

We and other groups reported that activation of FGF signaling by microinjection of FGF-2 into the lateral ventricles of the brain or by constitutively active mutations of FGF receptor 3 results in proliferation of NPCs and subsequent ventriculomegaly without any evidence of ventricular system stenosis (Inglis-Broadgate et al., 2005; Naruse et al., 2006; Rash et al., 2013). In addition, modifications of signaling pathways that are involved in the expansion of the NPC population also cause ventriculomegaly (Chenn and Walsh, 2003; Chizhikov et al., 2019; Roy et al., 2019). Interestingly, gyrification in lissencephalic mouse brains was occasionally observed in these mice. These findings suggest that extensive proliferation of NPCs, especially intermediate progenitor cells, during development is a key factor underlying the evolution from lissencephalic to gyrencephalic brains. In human and macaque monkey brains, expansion of the outer SVZ, comprising outer radial glia and intermediate progenitors, forms the cellular basis for production of massive numbers of neurons as well as cortex gyrification (Molnár et al., 2019). However, the roles of *KLF5* in the production and expansion of the intermediate progenitor population in primate neurogenesis and in the evolution of species having a gyrified cortex remain an open question.

References

Aksoy I, et al. (2014) Klf4 and Klf5 differentially inhibit mesoderm and endoderm differentiation in embryonic stem cells. Nat Commun 5:3719.

Amatsubo T, et al. (2009) Trifluoromethoxy-benzylated ligands improve amyloid detection in the brain using ^{19}F magnetic resonance imaging. Neurosci Res 63:76–81.

Anders S, Pyl PT, Huber W (2015) HTSeq–a Python framework to work with high-throughput sequencing data. Bioinformatics 31:166–169.

Artavanis-Tsakonas S, Matsuno K, Fortini ME (1995) Notch signaling. Science 268:225–232.

Azami T, et al. (2017) Klf5 maintains the balance of primitive endoderm versus epiblast specification during mouse embryonic development by suppression of Fgf4. Development 144:3706–3718.

Belenguer G, Duart-Abadia P, Jordán-Pla A, Domingo-Muelas A, Blasco-Chamarro L, Ferrón SR, Morante-Redolat JM, Fariñas I (2021) Adult neural stem cells are alerted by systemic inflammation through TNF-α receptor signaling. Cell Stem Cell 28:285–299.

Bialkowska AB, Yang V, Mallipattu SK (2017) Krüppel-like factors in mammalian stem cells and development. Development 144:737–754.

Bourillot PY, Savatier P (2010) Krüppel-like transcription factors and control of pluripotency. BMC Biol 8:125.

Bruce SJ, Gardiner BB, Burke LJ, Gongora MM, Grimmond SM, Perkins AC (2007) Dynamic transcription programs during ES cell differentiation towards mesoderm in serum versus serum-free BMP4 culture. BMC Genomics 8:365.

Chen Y, Lun AAT, Smyth GK (2016) From reads to genes to pathways: differential expression analysis of RNA-seq experiments using Rsubread and the edgeR quasi-likelihood pipeline. F1000Res 5:1438.

Chenn A, Walsh CA (2003) Increased neuronal production, enlarged forebrains and cytoarchitectural distortions in β-catenin overexpressing transgenic mice. Cereb Cortex 13:599–606.

Chizhikov VV, Iskusnykh IY, Steshina EY, Fattakhov N, Lindgren AG, Shetty AS, Roy A, Tole S, Millen KJ (2019) Early dorsomedial tissue interactions regulate gyrification of distal neocortex. Nat Commun 10:5192.

Dang DT, Chen X, Feng J, Torbenson M, Dang LH, Yang VW (2003) Overexpression of Krüppel-like factor 4 in the human colon cancer cell line RKO leads to reduced tumorigenecity. Oncogene 22:3424–3430.

Daun KA, Fuchigami T, Koyama N, Maruta N, Ikenaka K, Hitoshi S (2020) Early maternal and social deprivation expands neural stem cell population size and reduces hippocampus/amygdala-dependent fear memory. Front Neurosci 14:22.

Ema M, et al. (2008) Krüppel-like factor 5 is essential for blastocyst development and the normal self-renewal of mouse ESCs. Cell Stem Cell 3:555–567.

Florek M, Haase M, Marzesco AM, Freund D, Ehninger G, Huttner WB, Corbeil D (2005) Prominin-1/CD133, a neural and hematopoietic stem cell marker, is expressed in adult human differentiated cells and certain types of kidney cancer. Cell Tissue Res 19:15–26.

Fuentealba LC, Rompani SB, Parraguez JI, Obernier K, Romero R, Cepko CL, Alvarez-Buylla A (2015) Embryonic origin of postnatal neural stem cells. Cell 161:1644–1655.

Furutachi S, et al. (2015) Slowly dividing neural progenitors are an embryonic origin of adult neural stem cells. Nat Neurosci 18:657–665.

Ghaleb AM, Nandan MO, Chanchevalap S, Dalton WB, Hisamuddin IM, Yang VW (2005) Krüppel-like factors 4 and 5: the yin and yang regulators of cellular proliferation. Cell Res 15:92–96.

Hansen D, Lui JH, Parker PRL, Kriegstein A (2010) Neurogenic radial glia in the outer subventricular zone of human neocortex. Nature 464:554–561.

Haubensak W, Attardo A, Denk W, Huttner WB (2004) Neurons arise in the basal neuroepithelium of the early mammalian telencephalon: a major site of neurogenesis. Proc Natl Acad Sci U S A 101:3196–3201.

Hevner RF (2019) Intermediate progenitors and Tbr2 in cortical development. J Anat 235:616–625.

Hitoshi S, Alexon T, Tropepe V, Donoviel D, Elia AJ, Nye JS, Conlon RA, Mak TW, Bernstein A, van der Kooy D (2002) Notch pathway molecules are essential for the maintenance, but not the generation, of mammalian neural stem cells. Genes Dev 16:846–858.

Hitoshi S, Seaberg RM, Koscik C, Alexson T, Kusunoki S, Kanazawa I, Tsuji S, van der Kooy D (2004) Primitive neural stem cells from the mammalian epiblast differentiate to definitive neural stem cells under the control of Notch signaling. Genes Dev 18:1806–1811.

Hitoshi S, Kippin T, van der Kooy D (2011) Culturing adult neural stem cells: application to the study of neurodegenerative and neuropsychiatric pathology. In: *Neurogenesis in the adult brain II: clinical implications* (Seki T, Parent JM, Alvarez-Buylla A, eds), pp 187–207. New York: Springer.

Inglis-Broadgate SL, Thomson RE, Pellicano F, Tartaglia MA, Pontikis CC, Cooper JD, Iwata T (2005) FGFR3 regulates brain size by controlling progenitor cell proliferation and apoptosis during embryonic development. Dev Biol 1:73–85.

Isaka F, Ishibashi M, Taki W, Hashimoto N, Nakanishi S, Kageyama R (1999) Ectopic expression of the bHLH gene Math1 disturbs neural development. Eur J Neurosci 11:2582–2588.

Ishino Y, et al. (2014) Bre1a, a histone H2B ubiquitin ligase, regulates the cell cycle and differentiation of neural precursor cells. J Neurosci 34: 3067–3078.

Jeon H, Waku T, Azami T, Khoa LTP, Yanagisawa J, Takahashi S, Ema M (2016) Comprehensive identification of Krüppel-like factor family members contributing to the self-renewal of mouse embryonic stem cells and cellular reprogramming. PLoS One 11:e0150715.

Jiang J, Chan YS, Loh YH, Cai J, Tong GQ, Lim CA, Robson P, Zhong S, Ng HH (2008) A core Klf circuitry regulates self-renewal of embryonic stem cells. Nat Cell Biol 10:353–360.

Kim D, Langmead B, Salzberg SL (2015) HISAT: a fast spliced aligner with low memory requirements. Nat Methods 12:357–360.

Kowalczyk T, Pontious A, Englund C, Daza RA, Bedogni F, Hodge R, Attardo A, Bell C, Huttner WB, Hevner RF (2009) Intermediate neuronal progenitors (basal progenitors) produce pyramidal-projection neurons for all layers of cerebral cortex. Cereb Cortex 19:2439–2450.

Liao Y, Smyth GK, Shi W (2014) Featurecounts: an efficient general purpose program for assigning sequence reads to genomic features. Bioinformatics 30:923–930.

Llorens-Bobadilla E, Zhao S, Baser A, Saiz-Castro G, Zwadlo K, Martin-Villalba A (2015) Single-cell transcriptomics reveals a population of dormant neural stem cells that become activated upon brain injury. Cell Stem Cell 17:329–340.

Love MI, Huber W, Anders S (2014) Moderated estimation of fold change and dispersion for RNA-seq data with DESeq2. Genome Biol 15:550.

McConnell BB, Ghaleb AM, Nandan MO, Yang VW (2007) The diverse functions of Krüppel-like factors 4 and 5 in epithelial biology and pathobiology. Bioassays 29:549–557.

Molnár Z, et al. (2019) New insights into the development of the human cerebral cortex. J Anat 235:432–451.

Moore DL, Apara A, Goldberg JL (2011) Krüppel-like transcription factors in the nervous system: novel players in neurite outgrowth and axon regeneration. Mol Cell Neurosci 47:233–243.

Nakamura Y, Sakakibara S-I, Miyata T, Ogawa M, Shimazaki T, Weiss S, Kageyama R, Okano H (2000) The bHLH gene Hes1 as a repressor of the neuronal commitment of CNS stem cells. J Neurosci 20:283–293.

Nandan MO, Yang VW (2009) The role of Krüppel-like factors in the reprogramming of somatic cells to induced pluripotent stem cells. Histol Histopathol 24:1343–1355.

Nandan MO, McConnell BB, Ghaleb AM, Bialkowska AB, Sheng H, Shao J, Babbin BA, Robine S, Yang VW (2008) Krüppel-like factor 5 mediates cellular transformation during oncogenic KRAS-induced intestinal tumorigenesis. Gastroenterology 134:120–130.

Naruse M, Nakahira E, Miyata T, Hitoshi S, Ikenaka K, Bansal R (2006) Induction of oligodendrocyte progenitors in dorsal forebrain by intraventricular microinjection of FGF-2. Dev Biol 297:262–273.

Ohnishi S, Ohnami S, Laub F, Aoki K, Suzuki K, Kanai Y, Haga K, Asaka M, Ramirez F, Yoshida T (2003) Downregulation and growth inhibitory effect of epithelial-type Krüppel-like transcription factor KLF4, but not KLF5, in bladder cancer. Biochem Biophys Res Commun 308:251–256.

Parisi S, Passaro F, Aloia L, Manabe I, Nagai R, Pastore L, Russo T (2008) Klf5 is involved in self-renewal of mouse embryonic stem cells. J Cell Sci 121: 2629–2634.

Pertea M, Pertea GM, Antonescu CM, Chang TC, Mendell JT, Salzberg SL (2015) Stringtie enables improved reconstruction of a transcriptome from RNA-seq reads. Nat Biotechnol 33:290–295.

Qin S, Zhang CL (2012) Role of Krüppel-like factor 4 in neurogenesis and radial neuronal migration in the developing cerebral cortex. Mol Cell Biol 32:4297–4305.

Ramírez F, Ryan DP, Grüning B, Bhardwaj V, Kilpert F, Richter AS, Heyne S, Dündar F, Manke T (2016) Deeptools2: a next generation web server for deep-sequencing data analysis. Nucleic Acids Res 44:W160–W165.

Rash BG, Tomasi S, Lim HD, Suh CY, Vaccarino FM (2013) Cortical gyrification induced by fibroblast growth factor 2 in the mouse brain. J Neurosci 33:10802–10814.

Robinson JT, Thorvaldsdóttir H, Turner D, Mesirov JP (2023) Igv.js: an embeddable JavaScript implementation of the integrative genomics viewer (IGV). Bioinformatics 39:btac830.

Roy A, Murphy RM, Deng M, MacDonald JW, Bammler TK, Aldinger KA, Glass IA, Millen KJ (2019) PI3K-Yap activity drives cortical gyrification and hydrocephalus in mice. Elife 8:e45961.

Sherman BT, Hao M, Qiu J, Jiao X, Baseler MW, Lane HC, Imamichi T, Chang W (2022) DAVID: a web server for functional enrichment analysis and functional annotation of gene lists (2021 update). Nucleic Acids Res 50:W216–W221.

Suske G, Bruford E, Philipsen S (2005) Mammalian SP/KLF transcription factors: bring in the family. Genomics 85:551–556.

Tanaka A, Ishida S, Fuchigami T, Hayashi Y, Kuroda A, Ikenaka K, Hitoshi S (2020) Life-long neural stem cells are fate-specified at an early developmental stage. Cereb Cortex 30:6415–6425.

Tetreault MP, Yang Y, Katz JP (2013) Krüppel-like factors in cancer. Nat Rev Cancer 13:701–713.

Tropepe V, Sibilia M, Ciruna BG, Rossant J, Wagner EF, van der Kooy D (1999) Distinct neural stem cells proliferate in response to EGF and FGF in the developing mouse telencephalon. Dev Biol 208:166–188.

Walker TL, Wierick A, Sykes AM, Waldau B, Corbeil D, Carmeliet P, Kempermann G (2013) Prominin-1 allows prospective isolation of neural stem cells from the adult murine hippocampus. J Neurosci 33:3010–3024.

Wang X, Tsai J-W, LaMonica B, Kriegstein A (2011) A new subtype of progenitor cell in the mouse embryonic neocortex. Nat Neurosci 14:555–561.

Willaime-Morawek S, Seaberg RM, Batista C, Labbé E, Attisano L, Gorski JA, Jones KR, Kam A, Morshead CM, van der Kooy D (2006) Embryonic cortical neural stem cells migrate ventrally and persist as postnatal striatal stem cells. J Cell Biol 175:159–168.

Yamane M, Ohtsuka S, Matsuura K, Nakamura A, Niwa H (2018) Overlapping functions of Krüppel-like factor family members: targeting multiple transcription factors to maintain the naive pluripotency of mouse embryonic stem cells. Development 145:dev162404.

Yoon K, Gaiano N (2005) Notch signaling in the mammalian central nervous system: insights from mouse mutants. Nat Neurosci 8:709–715.